KASDI MERBAH OUARGLA UNIVERSITY
Faculty of Applied Sciences
Department of Electrical Engineering

FINAL STUDY DISSERTATION
In the aim of obtaining MASTER Degree ACADEMIC
Domain : Science and Technology
Option : Electrical Engineering
Specialty : Industrial Electrotechnics

Presented by :
Bouaka Mohammed Fateh
Beggui Abdelkader

Theme:

Optimization by simulation of a thin film solar cell based on antimony sulfide selenide $Sb_2(Se_{1-x}S_x)_3$

Publicly debated on: 11 / 06 / 2022 in front of the examining committee
Composed of:

Mr Djafour Ahmed	Professor	President	UKMOuargla
Mr Bouhafs Ali	MAA	Examiner	UKM Ouargla
Mr BenmirAbdelkader	MCB	Supervisor	UKM Ouargla

Academic year: 2021/2022

DEDICATION

We dedicate this modest work to those who are the source of our inspiration and our courage.

To my dear mother, who always gives me hope to live and who has neverstopped praying for me.

To my dear father, for his encouragement and support, and above all forhis sacrifice so that nothing will hinder The course of my studies.

To all the professors and teachers who have followed me throughout myschooling and who have allowed me to succeed in my studies.

To my dear brothers

All my friends

Acknowledgments

First of all, we thank ALLAH for having given us the courage and patience to arrive at this modest work.

We would like to thank our supervisor Dr. Benmir Abdelkader, who hasbeen always generous during all phases of the research, his follow-up and advice throughout this period.

Our gratitude also goes to the members of the jury who accepted to examine and evaluate my work. We thank heartily Mr Djafour Ahmed. We thank greatly Mr Bouhafs Ali

Our most grateful thanks to all those who have contributed to the realization of this memory.

Finally, we would like to express our tremendous gratitude to our family and our friends for their support during these years.

Abstract

The aim of this work is to optimize by simulation a thin-film solar cell based on$Sb_2(Se_{1-x}S_x)_3$. The simulation was carried out by SCAPS software. It was found that a maximum conversion efficiency of the cell η = 8.21% was obtained for an optimal value of thickness of the absorber layer of 0.2 µm. Whereas, the optimal composition Y of this layer is the lowest, which corresponds to the lowest value of the gap, Eg = 1.18 eV. While, the concentration of the doping atoms of this absorber layer does not exceed Na=$10^{15}cm^{-3}$. Moreover, this absorber layer must be chosen in such a way that it contain the lowest possible density of defects.

الملخص

الهدف من هذا العمل هو التحسين عن طريق المحاكاة لخلية شمسية رقيقة تعتمد على $Sb_2(Se_{1-x}S_x)_3$. تمت المحاكاة بواسطة برنامج SCAPS . وجد أنه تم الحصول على أقصى كفاءة تحويل للخلية η = 8.21 ٪ مقابل قيمة مثلى لسمك الطبقة الماصة تساوي 0.2 µm. في حين ، أن التركيب Y الأمثل هو الأدنى ، والذي يتوافق مع أدنى قيمة للفجوة Eg= 1.18 eV . بينما لايتجاوز تركيز ذرات المنشطات لهذه الطبقة Na=$10^{15}cm^{-3}$. علاوة على ذلك ، يجب اختيار هذه الطبقة الماصة بحيث تحتوي على أقل كثافة ممكنة من العيوب.

Résumé

L'objectif de ce travail est d'optimiser par simulation une cellule solaire à couches minces à base de $Sb_2(Se_{1-x}S_x)_3$. La simulation a été réalisée par le logiciel SCAPS. Il a été constaté qu'un rendement de conversion maximal de la celluleη = 8.21% a été obtenu pour une valeur optimale d'épaisseur de la couche absorbeur de 0,2 µm. Alors que, la composition Y optimale de cette couche est la plus faible, ce qui correspond à la plus faible valeur du gap, Eg = 1,18 eV. Tandis que, la concentration des atomes du dopage de cette couche absorbeur ne dépasse pas Na= $10^{15}cm^{-3}$. De plus, cette couche absorbeur doit être choisie de manière à ce qu'elle contienne la plus faible densité de défauts possible.

List of Figures

List of Tables

List of symbols

I_{cell}: cell current in darkness.

I_D: diode current.

I_0: saturation current.

k: Boltzmann constant.

q: charge of the electron (1, 6.10^{-19} C).

T: junction temperature in K°. ($1{,}38.10^{-23}$ j/K).

V_D: voltage applied on the diode.

I_{ph}: is the photocell current, proportional to illumination.

R_s: series resistance.

R_{sh}: shunt resistance.

I_{sc}: short-circuit current

V_{oc}: Open circuit voltage

P: power

FF: Fill factor

MPP: Maximum power

I_{MPP}: MPP current

V_{MPP}: MPP voltage

Ψ: potential

Contents

General introduction

General introduction

Energy is an essential component of economic growth and development, where its demand increases with the corresponding increase in population. Energy from fossil fuels such as oil, gas, and coal and water has been used to generate electricity on a large scale.

To manage the major problems of global warming, today's world needs renewable, cost-effective, and clean energy. Solar energy is the most abundant free resource available to us. It is a natural and safe alternative to non-renewable energies.

Energy solar photovoltaic (PV) is the electrical energy generated by the direct conversion of solar radiation using a device called a photovoltaic solar cell. Solar cells have the advantage of being clean, quiet, elegant and without rotating parts.

The ultimate research goal is to develop a solar cell that can simultaneously meet the so-called golden- triangle requirements: low cost, high power conversion efficiency (PCE) and long-term stability. Despite their increasing efficiency, c-Si-solar cells have not yet reached typical household applications due to their higher prices.

In recent years, thin-film solar cell efficiency such as those based on $Cu(In,Ga)Se_2$ (CIGS) and CdTe, are able to reduce the cost and they achieved PCE of around 22%. However, the scarcity of In, Ga, and Te on earth as well as the toxicity of Cd may limit their terawatt scale production.

In the last few years, antimony sulfide selenide $Sb_2(Se_{1-x}S_x)_3$ semiconductor has received considerable attention as an attractive absorber material in the thin-film hetero junction photovoltaic device due to its high absorption coefficient ($>10^5$ cm^{-1}),suitable tunable bandgap ranging from 1.1 to 1.7 eV, low-cost, earth-abundant, low-toxicity, low temperature fabrication process and air-stable materials.

Numerical simulation is a useful tool for predicting the effect of changes in material proprieties, measure the potential merits of cell structures and then optimizing cell structure.

In this work, we will use Solar Cell Capacitance Simulator (SCAPS) to optimize a set of physical and geometric parameters such as the thickness of absorber layer, composition ratio (bandgap), doping density and defect density.

This work is organized as follows:

- In the first chapter, we call upon some useful notions in the field photovoltaic (PV) solar cells;
- The second chapter is devoted to a more accurate study of the material$Sb_2(Se_{1-x}S_x)_3$, which is the absorber layer of the solar cell PV;
- In the third chapter, we present the basic equations of the model used by SCAPS software. Next, we will describe the simulation method by this program. Then, we optimize some physical and geometric parameters of the $Sb_2(Se_{1-x}S_x)_3$ absorber layer of a thin film solar cell;
- Finally, we will conclude with a general conclusion.

Chapter I

Generalities on Photovoltaic Solar Cells

Chapter I: Generalities on Photovoltaic Solar Cells

I. 1. Introduction

In this first chapter, we call upon some useful notions in the field photovoltaic (PV) solar cells. First, we start with a history of PV solar cells and a brief overview of solar radiation. Then we will define the PV solar cell. Then we detail the operating principle of this cell and its equivalent circuit and its main PV characteristics. Finally, we briefly explain the different generations of PV solar cells.

I. 2. Brief History of Solar Cells

Solar cell, also known as a photovoltaic (PV) cell, harvests sunlight and transfers the energy into electricity by the photovoltaic effect. The term "photovoltaic" is based on the Greek word photos(meaning "light") and the word "voltaic" (meaning "electric"), which comes from the name of the Italian physicist Alessandro Volta, after whom the unit of electric potential, the volt, is named. The photovoltaic effect was discovered in 1839 by the French physicist Alexandre-Edmond Becquerel. More than 40 years later, in 1883, the first solar cell was built by an American, Charles Fritts, who coated selenium with a very thin layer of gold to form junctions, resulting in efficiency of only 1%. Then, in 1941 Russell Ohl built the first silicon-doped solar cell. The modern age of solar power technology arrived in 1954 when Bell Laboratories, experimenting with semiconductors, accidentally found that silicon doped with certain impurities was very sensitive to light. Daryl Chapin, Calvin Souther Fuller, and Gerald Pearson of Bell Laboratories then developed the first silicon solar cell capable of converting sunlight energy into enough power to run every day electric equipment , with efficiency of about 5% [1].

I. 3. Solar Spectrum

The study of solar cells (progress, optimization and characterization….etc.) need some information about the source of energy used; the sun. This star is the biggest member of the solar system. The sun is a big sphere of plasma composed of H and He and some small amounts of other elements, it has an effective blackbody temperature T_S of 5777 K. The diameter of the sun is around $1.39x10^6$km and the distance between it and the earth is about $1.5x10^8$km. The solar radiation is partially absorbed and scattered by its passage

through the atmosphere. The absorption of the X–rays and extreme ultraviolet radiations of the sun is principally caused by nitrogen and oxygen while the absorption of the ultraviolet (λ<0.40 μm) and infrared radiations (λ>2.3 μm) is mainly caused by the ozone and water vapors. The atmosphere of the earth absorbs the ultraviolet (UV) and far infrared radiation and allows only short wavelength radiation (i.e. between 0.29 μm and 2.3 μm). It does not permit radiation having wavelength λ>2.3 μm, (i.e. long wavelength radiation) [2]. (Figure I-1) shows the solar spectrum as a function of photon energy. The terms AM0 and AM1.5 used in this figure are the designations of a particular radiation conditions. The concept , "Air Mass (AM)" represents the amount of atmosphere through which the solar radiation has travelled and is correlated to the amount of absorption.

$$\mathbf{AM} = \frac{\mathbf{1}}{\mathbf{cos(\theta)}} \qquad \textbf{(I-1)}$$

The θ represents the angle of the sun to the vertical. Outside the atmosphere, the spectrum is AM0 and that on the surface of the earth for normal incidence is AM1. The spectrum AM1.5 corresponds to an angle of incidence of solar radiation of 48° relative to the surface normal. This energy spectrum is regarded as the standard spectrum for measuring the efficiency of PV cells used for terrestrial applications.

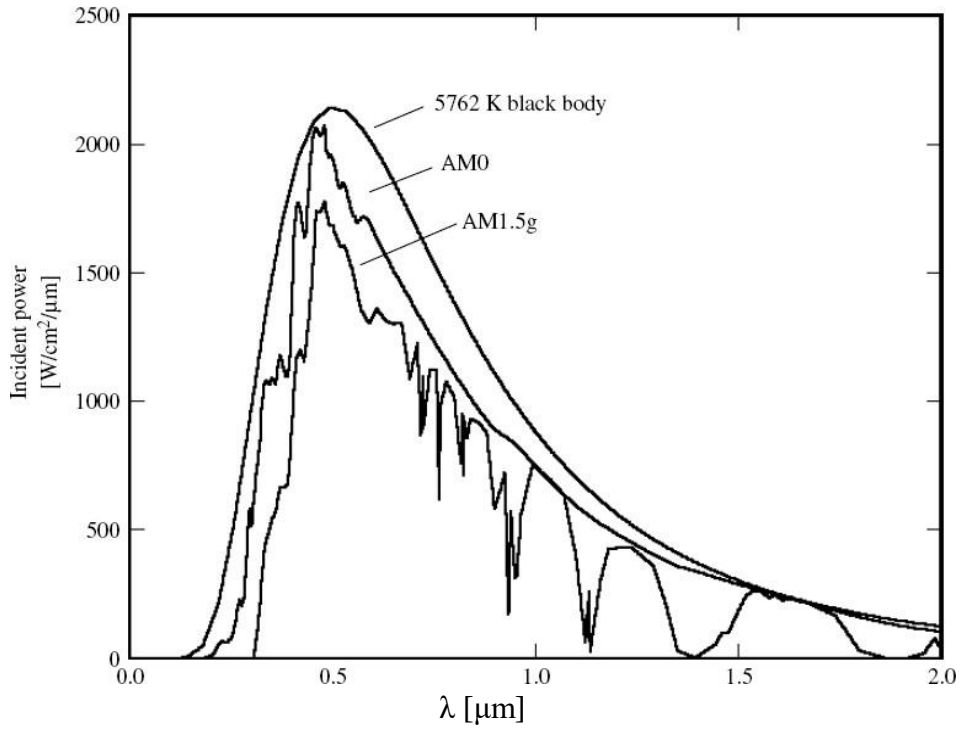

Figure I-1 - Solar spectrum for different Air Mass and blackbody radiation corresponding to the sun.

I. 4. Photovoltaic cells

The photovoltaic cells are semiconductor devices; they are usually made of silicon in its various forms. They do not implement any fluid and do not contain corrosive substances and no mobile piece [3]. They produce electricity as long as they are exposed to solar radiations [4]. They do not require virtually no maintenance; they do not pollute and produce no noise. Photovoltaic cells are thus the safest and most ecologically to produce energy [3].

I.4.1.PV cell structure and operating principle

I. 4. 1. 1. PV cells structure

The basic structure of a PV cell is a PN junction consisting of the follow (Figure I-2): a P-doped semiconductor crystal is covered with a thin doped region [5]–[6]. Between the two areas develops a junction. The area N is covered by a metal grid that serves as the cathode, while a metal plate covers the other face of the crystal and plays the role of anode. The total thickness of the crystal is of the order of a millimeter [7,8].

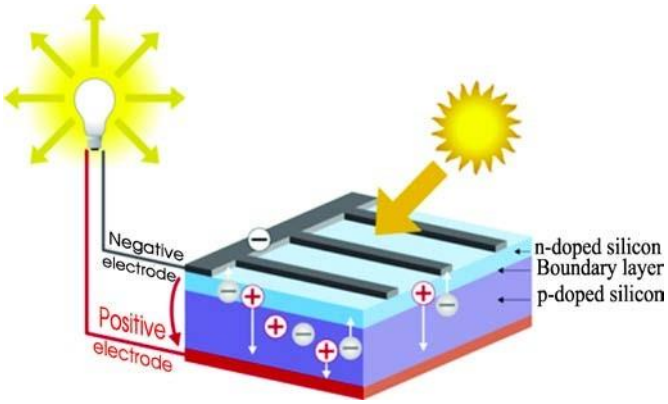

Figure I-2- Basic structure of a solar cell [9]

I. 4. 1. 2. Operating principle

A solar cell is an electronic component that converts sunlight into electricity. Its operating principle based on the photovoltaic effect involves three physical phenomena, simultaneous [10], can be described by the following mechanisms:

a). Absorption of incident photons (optical absorption) and creation of electron-hole pairs if the incident photon energy is greater than the gap of the material;

b). Diffusion of minority charge carriers to the space charge zone. Transfer of electric charges in the area where they will be the majority, through the electric field that present in the space charge region of the PN junction and collect. During the diffusion of charges to

the space charge zone, the electric charges can recombine and be lost;

c). Power dissipation in the load and in the parasitic resistances.

It is therefore essential that the material used possesses specific optical and electrical properties to enable photovoltaic conversion [5].

I. 4. 2. Photovoltaic cell characteristics

The photovoltaic cells are similar to a PN diode by its constitution, the materials used, and identical physical phenomena implemented. The behavior of a PV cell can be modeled like a poor PN junction as much static that in dynamic when this last is not illuminated [11]. The expression of the photovoltaic cell in this case is exactly like the famous expression of silicon diode in darkness [11]:

$$\mathbf{I_{cell}=I_D=I_0\left[\left(e^{\frac{qV_D}{KT}}\right)-1\right]} \qquad \textbf{(I-2)}$$

With:

I_{cell}: Cell currant in darkness.

I_D: Diode current.

I_0: Saturation current dependent on the temperature T and electrical and technological parameters of the PN junction [12].

K: Boltzmann constant.

q: Charge of the electron (1, 6.10^{-19} C).

T: Junction temperature in K (1,38.10^{-23} J/K).

V_D: Voltage applied on the diode.

Under illumination, the expression (I-2) will be as follow [10]:

$$\mathbf{I_{cell}=I_{ph}-I_D=I_{ph}-I_0\left[\left(e^{\frac{qV_{cell}}{KT}}\right)-1\right]} \qquad \textbf{(I-3)}$$

Where: I_{ph} is the photocell current, proportional to illumination.

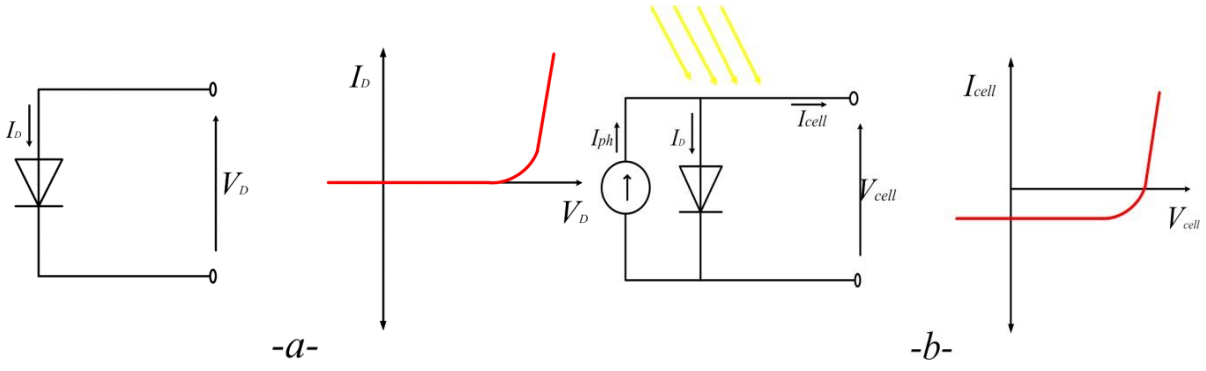

Figure I-3- Schematic of ideal photovoltaic cell

a: without illumination, b: with illumination

To reflect the current generated by the illuminated cell and different losses of connectivity that modeled by resistances, two terms are added R_s and R_{sh} (Figure I-4).

Therefore, output cell current [10] can be expressed as below:

$$\mathbf{I_{cell} = I_{ph} - I_0 \left[\left(e^{\frac{q(V_{cell}+R_s I_{cell})}{KT}}\right) - 1\right] - \frac{(V_{cell}+R_s I_{cell})}{R_{sh}}} \qquad \mathbf{(I\text{-}4)}$$

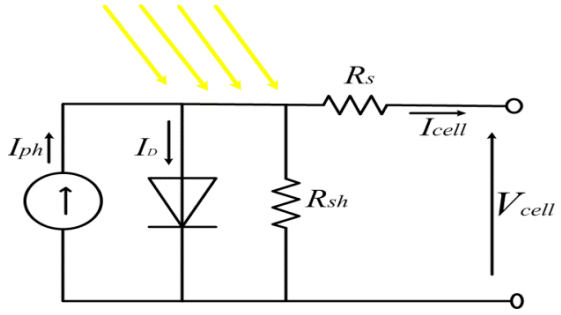

FigureI-4 - Schematic of real photovoltaic cell.

With:

R_s: Series resistance.

R_{sh}: Shunt resistance.

I. 4. 3. The important parameters of PV cells

The important parameters of PV cells are could be obtained from I-V curves, that is to say from the equation (I-4). The most common parameters are the following:

a) Short-circuit current I_{sc}

The short-circuit current I_{sc} of the dipole is the current that would cross it if its terminals were connected by perfect conductor of zero resistance. In the ideal case (R_s is null, R_{sh} is infinite), we need to impose the voltage V_{cell} zero in equation (I-4) to get I_{sc} equation. The equation of short-circuit current it will be as follow [10]:

$$\mathbf{I_{sc} = I_{ph}} \qquad \mathbf{(I\text{-}5)}$$

b) Open circuit voltage V_{oc}

It is the voltage across the cell when the latter is in open circuit, that is to say when the positive pole and the negative pole are electrically isolated from other electrical circuits (the current passing through it is zero). In this case, the power supplied by the cell P = V× I is zero. We need to impose the current I_{cell} zero in equation (I-4) to get V_{oc}.

The equation of the open circuit voltage in the ideal case is as follow:

$$\mathbf{V_{oc} = \frac{K.T}{q} \ln\left(\frac{I_{ph}}{I_0} + 1\right)} \quad \textbf{(I-6)}$$

c) Fill factor FF

It is the ratio between the maximum power delivered by the cell on the product of the short circuit current and open circuit voltage (Isc×Voc).

The equation of the factor is as follow [10]:

$$\mathbf{FF = \frac{I_{MPP} \times V_{MPP}}{I_{SC} \times V_{OC}}} \quad \textbf{(I-7)}$$

d) The efficiency

It is the ratio between the energy provided and the incident light power P_{in}. This measurement is done under standard illumination and temperature conditions.

The equation of the efficiency is as follow [10]:

$$\boldsymbol{\eta = \frac{P_{MPP}}{P_{in}} = \frac{FF \times I_{SC} \times V_{OC}}{P_{in}}} \quad \textbf{(I-8)}$$

I.5.Types of Solar Cells

The solar cell technology is very rich corresponding to substance used and production type. There are more than dozen of substances besides lots of them are being working progress in order to produce a solar cell.

Solar cells can be categorized in three parts [13]:

- First Generation Solar Cells: Crystalline Silicium
- Second Generation Solar Cells: Thin Film
- Third Generation Solar Cells: Nanotechnology based solar cells

I. 5. 1. First generation solar cells

I.5.1.1. Crystalline silicium solar cells

Silicium is a substance that typically shows semi-conductor properties and one of the most commonly using materials in production of a solar cell. Besides it looks like it will keep its position because of superiority of its technology and economic reasons however there are other substances has photovoltaic properties. Usually, a standard lifetime of crystalline solar cell is represented as 25 years. Ideal work temperature is about 25 degrees Celsius.

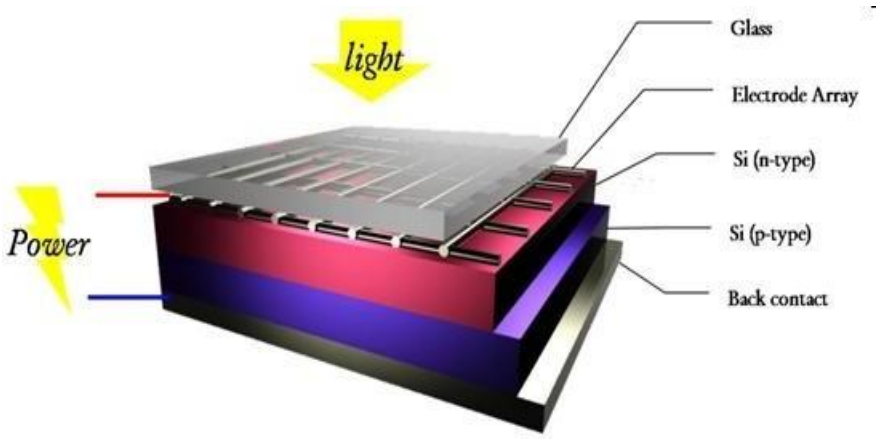

Figure I-5- First Generation Solar Cell [14].

I.5.1.2. Mono-crystalline silicium solar cells

This type of solar cell first obtains with a method that is called CHROZALSKI crystal pulling method. It is still most using method in photovoltaic industry. In this method silicium oxide goes through a phase with some chemicals in arc ovens to get pure silicium. After that a silicium particle called core or seed sops into this solution. When core pulled out from the cold solution, it will all over the core. After the silicium became bullion, it cut into slices with a cutter. It will be after these two processes. First bullion cut as rectangular blocks and then these blocks are handling as a battery. Laboratory efficiency is about 26%.

I.5. 1.3.Poly-crystalline silicium solar cells

This type is made from ribbon silicium technology and their structure shows polycrystalline properties. Laboratory efficiency is about 23 %. Their prices are low because of the production cost.

I.5.2. Second Generation (Thin Film) Solar Cells

In this technic, aim is the reduce thickness of the cell with using substances which has higher quality to absorb light. Absorption coefficient of amorphous silicium solar cells is greater than crystalline type solar cells' coefficient. For example, even 1 micron thick amorphous silicium can absorb the light radiation in a region with wavelength is 0.7 µm , to absorb the same light crystal silicium has to be at 500 microns thick. Therefore, amorphous silicium has advantage because using less material for made.

I.5.2.1. Amorphous Silicium Solar Cells

Amorphous silicium solar cells are the primary sample of thin film technology of solar cells. However, first made (a-Si) solar cells are in Schottky barrier structure, then p-i-n junction structures are developed. Laboratory efficiency is about 10%. High costs materials are needed during fabric phase but sometimes firms prefer this type because of production duration is cheap.

I.5.2.2. Copper indium gallium diselenide Solar Cells

This type of solar cells consists of coming together elements in first, third and sixth groups of periodic table. Its absorption coefficient is very high. This compound (CIS) is made of from copper, indium, and selenium are called as CIS solar cells. With the contribution of the gallium in the compound obtained greater efficiency. However, as increase in the number of elements in the compound makes situation complex to control properties or contributions of elements for the system. Laboratory cell efficiency is about 23 %. There are two methods in production, first vaporizing the elements in a vacuum simultaneously. Second, reacting the copper indium thin film alloy with selenium in a suitable environment, which is also called selenization. In both cases, purpose is to establish a diode between the plates.

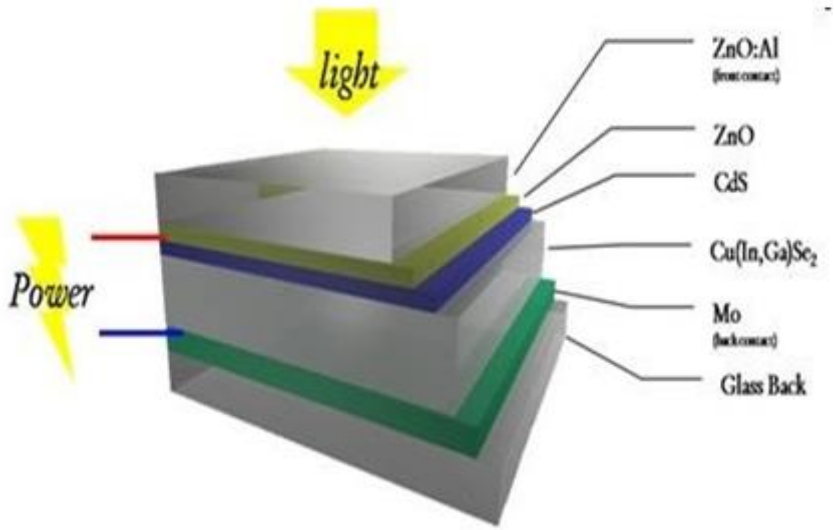

Figure I-6 - Second Generation Solar Cell [14].

I.5.2.3.Cadmium Telluride Solar Cells

This type of solar cells is made with simple methods and they are cheap. It has the shortest energy payback time of all solar technologies. However, experimental efficiency is up to 22 %.

I.5.3.Third Generation Solar Cells

Third Generation or as known as multi-junction solar cells enhance poor electrical performance while maintaining very low production costs. Current researches are targeting conversion efficiencies of 30% - 60% while retaining low cost materials and manufacturing techniques. However, these researches are still ongoing for this technology and there are no solid conclusions so far. It will be big progress about energy subject if they are in fabric because they submit super high value efficiency comparing to present ones.

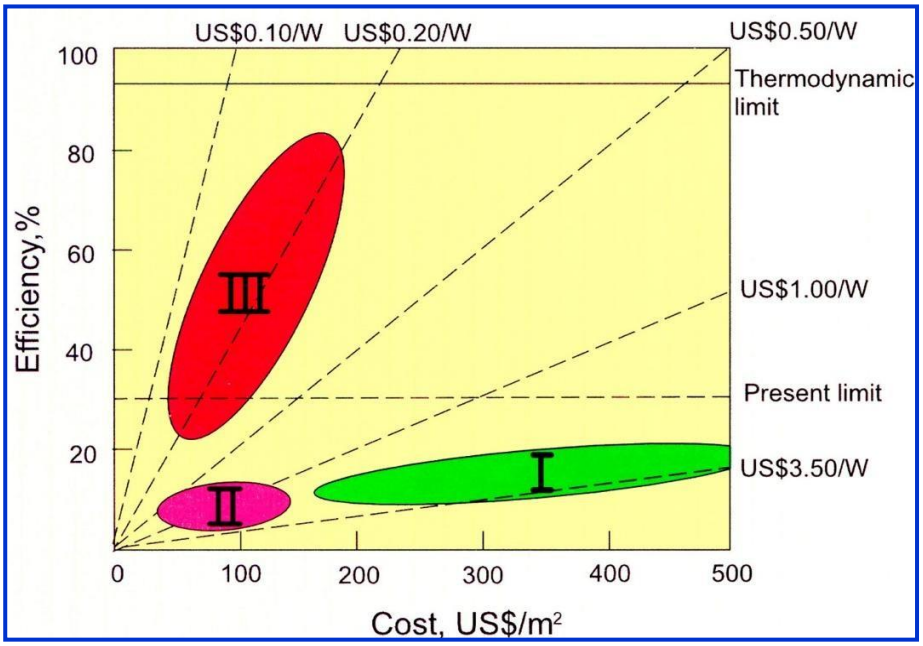

Figure I-7 - The Efficiency and product cost comparison of All Generations [15].

I.5.3.1.Super tandem Cells

This type of solar cells is combined of other type of solar cells, which has different energy spectrum to utilize sunlight's large energy spectrum. It also use lens sort of a magnifying glass. Theoretically, they have 86% efficiency but for obtained result for a sample of 1 cm² cell type the value is about 35%. Until now, these tandems cells have been producible only by using very special, expensive semi-conductor materials, and at very high costs.

I.5. 3.2.Intermediate Solar Cells

Solar cell materials with more than one bandgap offer the possibility to increase the efficiency of the solar cell beyond that of a single bandgap cell. According to this expression, intermediate band solar cell is one such possibility, where an intermediate

energy band is placed in the otherwise forbidden bandgap of the solar cell material. Having the ideal bandgaps efficiency can be 63.2%. Ordinary single bandgap cell has an efficiency limit 40%. However, even since for Intermediate solar cells there is no accessible efficiency value.

I.6.Conclusion

This chapter serves as a starting point for familiarization with the field photovoltaic. We started by describing solar radiation Then we mentioned the principle of operation of the photovoltaic cell and its different photovoltaic characteristics, and finally we briefly explain the different generations of photovoltaic cells.

Chapter II

Thin film solar cells based on

$Sb_2(Se_{1-x}S_x)_3$

Chapter II: Thin film solar cells based on $Sb_2(Se_{1-x}S_x)_3$

II. 1. Introduction

Among thin-film photovoltaic (PV) devices, CdTe, $Cu_2(In,Ga)Se_2$ (CIGS) and Perovskite solar cells have achieved impressive progresses, with decent efficiencies of 22.1%, 23.35%, and 25.2%, respectively [16]. Antimony chalcogenides, as an environmental-friendly and earth abundant light-absorber material with long-term stability for thin-film PV applications, have recently been proved to be an emerging inorganic candidate as the solar cell absorber. The family of antimony chalcogenide binary compounds employs the chemical formula of Sb_2X_3, including Sb_2S_3, Sb_2Se_3 and mixed chalcogenide $Sb_2(S,Se)_3$[17]. Sb_2X_3 possesses a unique one-dimensional (1D) crystal structure, bandgap in the range of 1.1 to 1.7 eV, high absorption coefficient ($> 10^5 cm^{-1}$ at visible wavelengths) and low melting points [18].

In this chapter, we start the properties and architectures of Sb_2X_3 solar cells, Installation of materials and construction of the device. We try to formulate Sb_2S_3, Sb_2Se_3 and $Sb_2(Se_{1-x}S_x)_3$ together as light absorber materials. Then we end up with the different constituent elements of the photovoltaic solar cell on $Sb_2(Se_{1-x}S_x)_3$.

II. 2. Properties of Sb_2X_3

Several typical fundamental properties of Sb_2X_3 are summarized in Table II-1, which are valuable to advance further development in photovoltaics.

During the last decade, Sb_2X_3 solar cells have experienced a significant increase in power conversion efficiency (PCE) from an initial value of below 1% to the record efficiency of 10.5% in 2020 [19]. In detail, the highest reported PCE of the planar-type and sensitized-type Sb_2S_3 solar cells are 7.1% and 7.5%, respectively [20,21], and the best Sb_2Se_3 solar cells gained the efficiencies of 9.2%, 3.21% for the planar-type and sensitized-type devices, respectively [22,23]. Regarding the $Sb_2(S,Se)_3$ solar cells, the planar-type, and sensitized-type devices reached the record efficiencies of 10.5% and 6.6%, respectively [19,24].

Property	Sb_2Se_3	Sb_2S_3
Lattice parameters		
a [Å]	11.6330	11.2285
b [Å]	11.7800	11.3107
c [Å]	3.9850	3.8363
Density [g cm^{-3}]	5.84	4.63
Melting point [K]	885	823
Band gap Eg (eV)		
Direct	1.03	1.84
Indirect	1.17	1.76
Absorption coefficient [cm^{-1}]	$> 10^5$	10^4-10^5
Relative dielectric constant ε_r	15.1	22
Exciton binding energy [eV]	1.28	-
Mobility [$cm^2V^{-1}S^{-1}$]		
μ_e	15	9.8
μ_h	42	10
Diffusion length [μm]	1.7	1
Minority-carrier lifetime [ns]	67	23

Table II-1 Electrical properties about antimony chalcogenide semiconductor materials [25].

II. 3. Device architectures

In general, antimony chalcogenide solar cells can be categorized into two types, mesoporous sensitized- and planar type. The planar-type structures can be further classified into two configurations, that is, substrate and superstrate.

II. 3. 1. Mesoporous sensitized-type structure

Sensitized-type Sb_2X_3 solar cells probably evolved from solid-state dye sensitized solar cells (DSSCs) [26,27]. As shown in Figure II-1-A, a compact TiO_2 layer is first deposited on a FTO or ITO substrate. As an electron transport layer, a thick layer of mesoporous TiO_2 scaffold is then spincoated onto the compact TiO_2 film. This scaffold is beneficial for electron extraction and play as a compensation for the short minority carrier (electron) diffusion lengths in Sb_2X_3 absorber. Once the Sb_2X_3 absorber layer infiltrated into these scaffolds, the Sb_2X_3 absorber layer is covered with a hole transport material (HTM). The thickness of HTM layer critically influences the efficient transportation and extraction of photogenerated carrier [28]. Finally, the metal electrode (e.g., Au or Ag) is prepared by evaporation.

II. 3. 2. Planar-type structure

Sensitized-type devices tend to have lower V_{Co} comparing with the planar-type devices. This should be attributed to the complex interface defects and charge recombination which occur at the mesoporous TiO_2/Sb_2X_3 interfaces [17, 29]. To solve this problem, the planar-type structure Sb_2X_3 solar cells eliminate the mesoporous layer, constructing a simpler device structure with reduced charge recombination channel. For the planar-type devices, it can be further separated into two main categories:

a). Superstrate configuration

In the superstrate Sb_2X_3 solar cells (Figure II-1-B), the device structure is composed of metal electrode (i.e., Au, Ag, Al, etc.), transparent conductive oxide (i.e., FTO and ITO), ETL (e.g., CdS, TiO_2, ZnO, SnO_2, etc.), HTL (e.g., Spiro-MeOTAD, P3HT, NiO_x, etc.) and Sb_2X_3 layers (e.g., Sb_2S_3, Sb_2Se_3 and $Sb_2(S,Se)_3$[30,31].

b).Substrate configuration

Another emerging architecture of Sb_2X_3 solar cells shown in Figure II-1-C is the substrate configuration, which, originated from CIGS device structure. A device configuration includes glass substrate/ metallic back-contact/HTL (e.g., $MoSe_2$)/Sb_2X_3 absorber layer/ETL (e.g., CdS, and $ZnSnO_4$, etc.)/ window layer (e.g., i-ZnO) /transparent electrode layer/Ni-Al grid electrode. So far, the highest PCEs of substrate configuration planar Sb_2S_3 and Sb_2Se_3devices are with 1.86% PCE and 9.2 % PCE, respectively [22,32].

Overall, the substrate structure allows the hetero junction to be optimized independently and there is no limitation for the substrate materials.

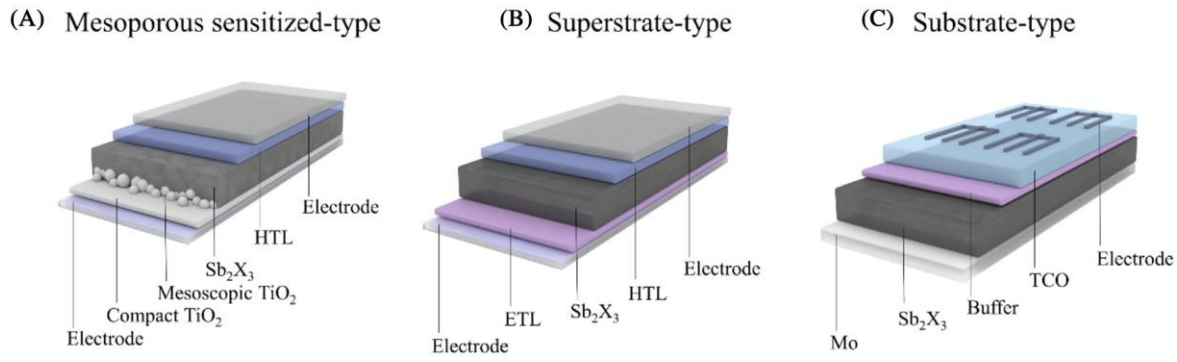

Figure II-1 Antimony chalcogenide solar cells configuration.

II.4.Materials properties of Sb_2S_3 and Sb_2Se_3

In specific, the elemental storage of Sb, S and Se in earth crust are 0.2, 260 and 0.05 ppm, respectively. The storage of Sb and S are considerably higher than those of In (0.049 ppm) and Te (0.005 ppm). This abundant storage set the basement for solar panel production in large scale at low cost, the relevant price and abundance of the corresponding elements are summarized in Figure II-2. In addition, not all of the three elements are included in the list of highly toxic or carcinogenic materials by Chinese, American as well as European Union regulation authorities. They can be regarded as environmental benign materials. In addition, they are binary compound. The controlling over the phase formation is not that rigorous. Furthermore, the melting points of $Sb_2S_3$and $Sb_2Se_3$are 500 and 608 °C, respectively, indicating low phase formation temperature required for the materials synthesis [33,34] .

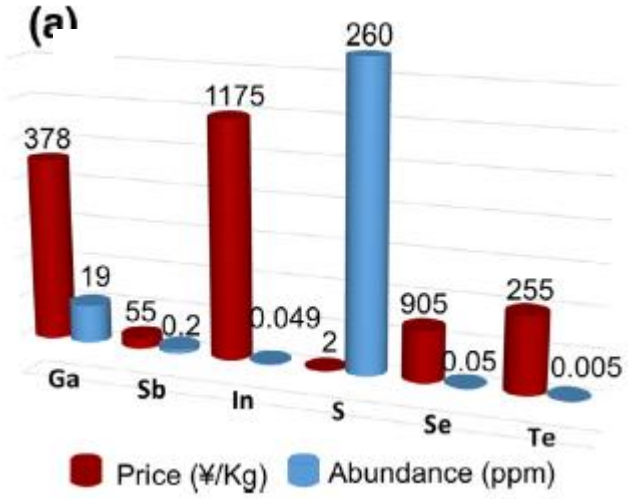

figure II-2 Price and earth abundance of Ga, Sb, In, S, Se, and Te.

II.4.1. Crystal structures of $Sb_2S_3$and Sb_2Se_3

$Sb_2S_3$and Sb_2Se_3 are nearly isomorphous; they crystallized in orthorhombic crystal structure [35,36].The anisotropic nature of Sb_2S_3 and Sb_2Se_3makes them tend to form 1D nanostructures, such as nanorod and nanoribbon [37–38].

For solar cell application, engineering the crystal structure with preferential alignment plays a critical role in the charge transport property and in turn determines the final photovoltaic performance.

II.4.2. Optoelectronic properties of $Sb_2(Se,S)_3$

According to the thermoelectric power measurement, Sb_2S_3 exhibits n-type conductivity, while Sb_2Se_3displays p-type conductivity [39]. The trap density for Sb_2S_3 films is Nt=1.69-2.2 $\times 10^{16}$ cm^{-3} for co-evaporated product and Nt=2.03–3.46× 10^{16} $cm^{-3}$for flash evaporated film sample [40]. In the chemical bath deposited (CBD) Sb_2S_3 films, the resistivity is 5.3 ×10^6cm, Hall mobility is 9.8 cm^2 V^{-1} s^{-1} and the carrier concentration is 1.2× $10^{12}cm^{-3}$. Importantly, both of Sb_2S_3 andSb_2Se_3 possess absorption coefficient ~10^5cm^{-1} in the ultraviolet and visible range, indicating that the film with thickness of several hundreds of nanomaters (e.g. ~500 nm) can harvest sufficient amount of light (e.g. ~90%) in the devices. A recent study shows that the electron diffusion length in Sb_2S_3falls into 290–900 nm [41].

II.5. Sb_2S_3based solar cells

Initial application of $Sb_2S_3$for photocurrent generation by Sb_2S_3can be dated back to 1992, when Savadogo and Mandal made photo electrochemical cells with 2.0% efficiencies under 40mWcm^{-2} illumination [42]. In 1994, the same group synthesizedSb_2S_3on Ge substrate by chemical bath deposition (CBD) approach, forming n-Sb_2S_3/p-Ge hetero junction solar cells [39]. To date, the applications of $Sb_2S_3$are generally based on either sensitized or planar hetero junction device architectures.

II.5.1. Sb_2S_3sensitized solar cells

The sensitized device structure is depicted in Figure II-3 (a), where Sb_2S_3de posited on the surface of TiO_2 nanoparticle network is applied as light harvester.

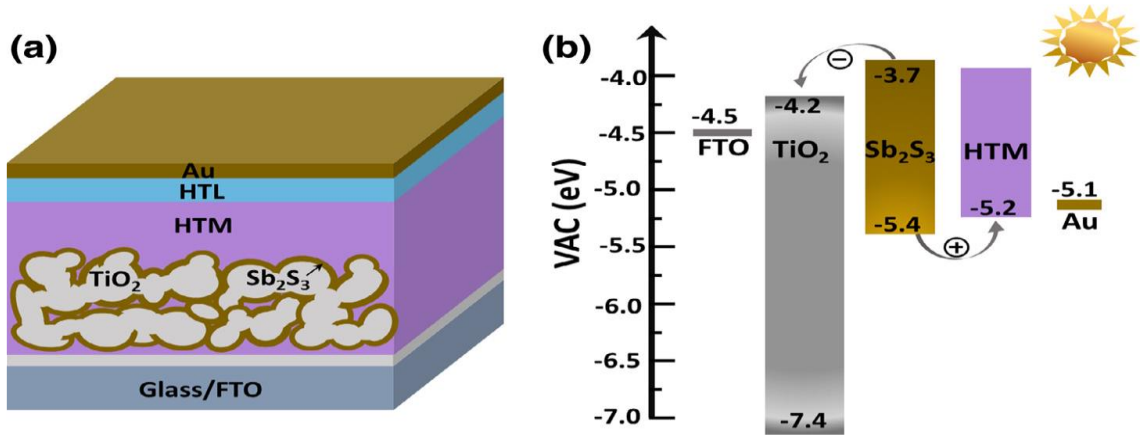

Figure II-3 (a) Schematic illustration of Sb_2S_3sensitized structure devices; (b) Simplified scheme of energy alignment versus vacuum of Sb_2S_3based solar cells.

Hole-transporting material (HTM) is infiltrated into the mesoporous network and attached onto the surface of Sb_2S_3. With that, the electron transports to the conduction band of TiO_2 and hole transports to the valence band of HTM (Figure II-3 (b)). It can also form so called extremely thin absorber (ETA) where a thin layer of Sb_2S_3 is adsorbed on the TiO_2 nanoparticle surface [43].

II.5.2. Sb_2S_3planar solar cells

Planar hetero junction solar cell not only simplifies the preparation process but also suppresses the generation of large amount of defects on mesoporous TiO_2nanoparticle surface.Efficiency is still relatively low (2.3%) in planar Sb_2S_3solar cells. Recently, a fast chemical approach (FCA) was developed to deposit Sb_2S_3 thin film on TiO_2blocking layer to build up planar hetero junction TiO_2/Sb_2S_3solar cell [33]. The device fabrication process is illustrated in Figure II-4. First, Sb_2O_3 was dissolved in CS_2 and butylamine to form a trans- parent precursor solution (Figure II-4 (a)). Afterwards, the solution was spin coated onto the substrate and annealed at 320 °C for only 2 min for the formation of Sb_2S_3 film.

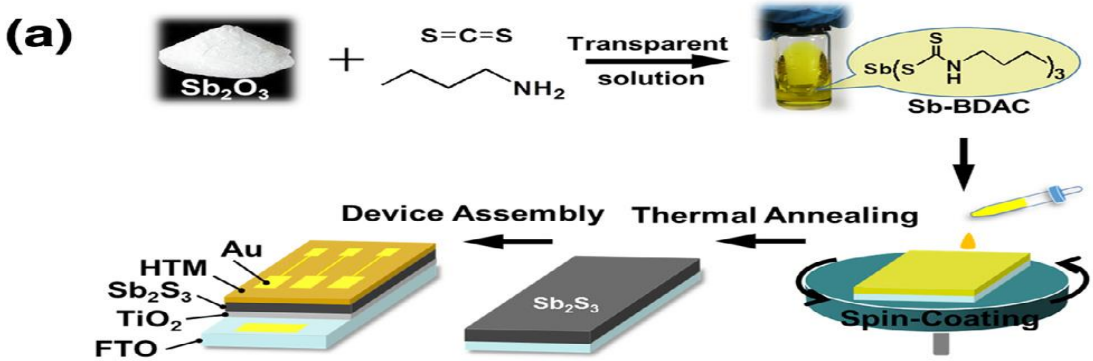

Figure II-4 (a) Illustration for the synthesis of Sb_2S_3 film and device assembly.

II.6. Sb_2Se_3based solar cells

Compared with Sb_2S_3, Sb_2Se_3 possesses narrower band gap of 1.1–1.3 eV, which is ideal for light absorption materials according to Shockley–Queisser theory [34]. Similar toSb_2S_3, the applications of Sb_2Se_3 for solar energy conversion are in either planar hetero-junction or sensitized device structures.

II.6.1. Sb_2Se_3 sensitized solar cells

In 2014, Seok and coworkers demonstrated Sb_2Se_3 - sensitized solar cell by spin-coating single-source precursor solution containing Sb and Se on mesoporous TiO_2 [34]. In this work, a PCE of 3.21% (V_{OC} = 304.5 mV, J_{SC} = 22.3mA cm^{-2} and FF = 47.2%) was achieved with the structure of FTO/ bl- TiO_2 /mp- TiO_2/Sb_2Se_3 /HTM/Au. Notably, Sb_2Se_3

was obtained at very low thermal decomposition and annealing temperature (200–300 °C) [44].

II.6.2. Sb_2Se_3 planar solar cells

There are considerable number of reports on the preparation of Sb_2Se_3 thin film, such as electrodeposition method, thermal evaporation method, SILAR and so on [45–46].

In this study, a PCE of 2.1% was achieved. Afterwards, a post-selenization process was utilized after thermal evaporation and the device efficiency was enhanced to 3.7% [47]. The oriented crystal growth perpendicular to the substrate facilitates charge transport and in turn suppresses the re- combination. By this method, the PCE of Sb_2Se_3 based planar hetero junction solar cell was stupendously improved towards 6.0% [48]. The buffer layers (CdS and ZnO) play a critical role in determining the device efficiency as well as stability. Randomly orientated ZnO prepared by spray pyrolysis dictates the growth of Sb_2Se_3 along orientation on ZnO substrate. Stimulated by the fabrication of CIGS thin-film solar cells, the Mai's group fabricated Sb_2Se_3 solar cell on the Mo substrate by co-evaporation of Se and Sb_2Se_3 [49]. Afterwards, the CdS was deposited onto the Sb_2Se_3 surface as window layer and ZnO and Al–ZnO were deposited sequentially to facilitate the charge extraction. Finally, a PCE of 4.25% was obtained. The co-evaporation of Se and Sb_2Se_3 is important for synthesizing high quality Sb_2Se_3 absorber film.

II.7.$Sb_2(Se_{1-x}S_x)_3$ based solar cells

Sb_2S_3possesses large band gap so that it can generate high V_{oc} in the devices. On the other hand, due to the large band gap, the light harvesting efficiency is limited. Sb_2Se_3 has smaller band gap of ~1.1eV, offering possibility for high photocurrent generation towards longer wavelength. However, the V_{oc} loss is significant. Taking advantages of the two materials is able to find an optimal absorbing material for efficient solar energy conversion. Since Sb_2S_3 and $Sb_2S_3$are isomorphous, the S atom in Sb_2S_3can be replaced by Se atom in a broad atomic ratio to form alloyed$Sb_2(S_{1-x}Se_x)_3$. Accordingly, a tunable bandgap can be obtained[44].

II.7.1. $Sb_2(Se_{1-x}S_x)_3$ sensitized solar cells

There are not too many reports on $Sb_2(Se_{1-x}S_x)_3$based sensi-tized solar cells. Recently, Seok's group reported a two-step fabrication of $Sb_2(Se_{1-x}S_x)_3$based inorganic–organic sensitized solar cells [24]. In this work, the precursor solution of $Sb_2Se_3$was spin-coated on the substrate of mesoporous TiO_2, followed by deposition of Sb_2S_3(Figure

II5(a)). This deposition process led to the formation of graded-composition of $Sb_2(Se_{1-x}S_x)_3$ upon annealing the stacking layers (Figure II-5 (a)). The graded-sensitizer with a stepwise composition from $Sb_2S_3$to Sb_2Se_3 showed favorable energy alignment (Figure II-5 (b) and (c)). With this kind of light absorption material, the solar cell gained a device PCE of 6.6%, the corresponding photovoltaic parameter of J_{sc}, $V_{oc}$and FF were 24.9 mA cm^{-2}, 474.8 mV and 55.6%, respectively. In the parallel study, the devices based on $Sb_2S_3$and Sb_2Se_3showed PCE of 5.3% and 2.7%, respectively, demonstrating the effectiveness of graded band structure for energy conversion [44].

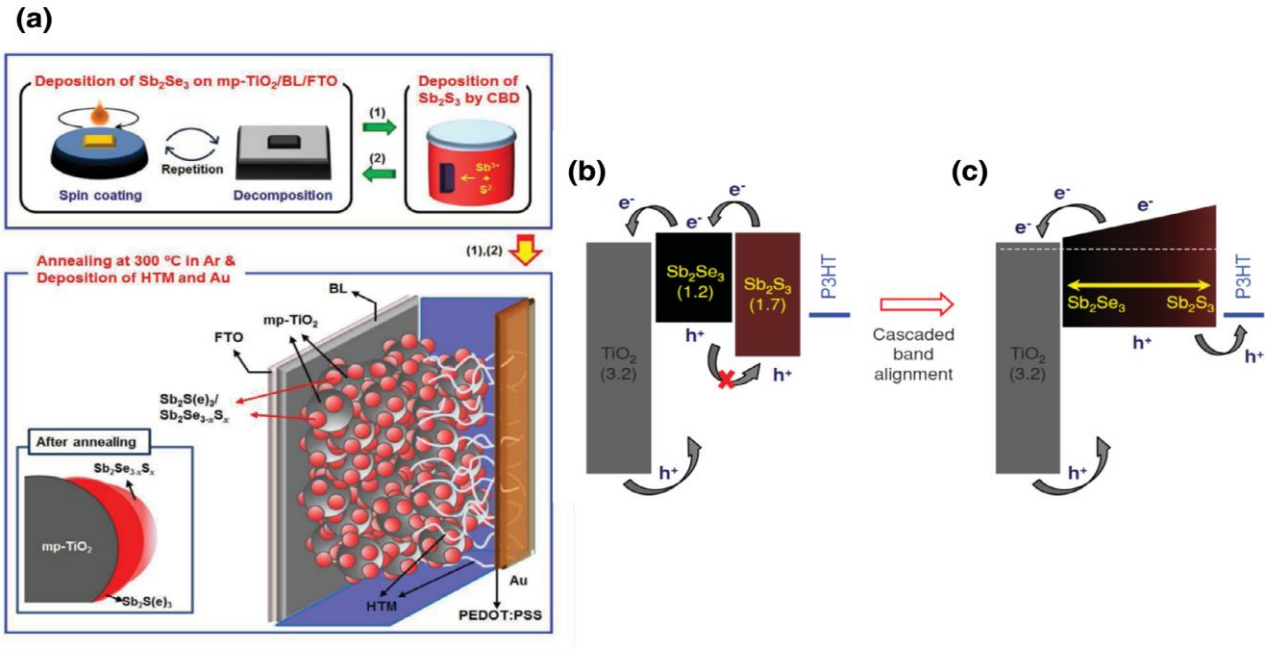

Figure II-5 (a) Schematic illustration of the fabrication process of the sensitized solar cells based on TiO_2/Sb_2Se_3 /Sb_2S_3 and $TiO_2/Sb_2S_3/Sb_2Se_3$structures; (b) Relative energy band diagram of TiO_2, Sb_2Se_3, $Sb_2S_3$and P_3HT; (c) Proposed cascaded-band alignment on the T/Se/S structure.

II.7.2.$Sb_2(Se_{1-x}S_x)_3$planar solar cells

Through introducing sulfur powder during RTE process, Tang's group prepared polycrystalline $Sb_2(S_{1-x}Se_x)_3$films with different S/Se ratios [50]. A device with TO/CdS/$Sb_2(S_{1-x}Se_x)_3$/Au gained a PCE of 5.79%. The methodology expanded the RTE method towards the fabrication of alloyed $Sb_2(Se_{1-x}S_x)_3$.It is proposed that the formation of graded band structure could generate internal electric field, which can enhance the charge separation and facilitate charge transport (Figure II-6 (a)). Finally, the device

delivered a PCE of 5.71% was obtained (Figure II. 6 (b)), which is essentially higher than the devices based on Sb_2S_3 and Sb_2S_3in parallel study [44].

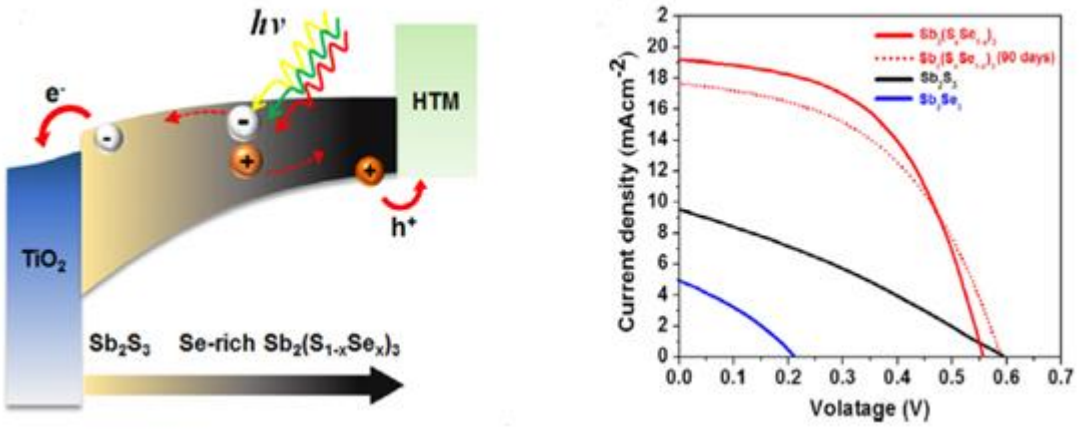

Figure II-6(a) Energy alignment diagram of corresponding materials used in device; (b)Typical current density–voltage curves of the devices based on different absorber materials.

II. 8.Physical Properties of $Sb_2(S_{1-x}Se_x)_3$Thin Films

The Sb_2S_3 and Sb_2Se_3 compounds are isomorphous and have the same orthorhombic crystalline structure (Figure II-7). A S atom can be replaced by a Se atom to build up the $Sb_2(S_{1-x}Se_x)_3$ternary compound. An important feature of the $Sb_2(S_{1-x}Se_x)_3$compound is the tunable bandgap that can be varied through the Se/ (S+Se) compositional ratio. The reported band-gap values for $Sb_2S_3$and Sb_2Se_3 are around 1.7 and 1.1 eV, respectively, thus a band-gap that lies between these two values can be obtained for the $Sb_2(S_{1-x}Se_x)_3$ compound (Figure II-8) [51].

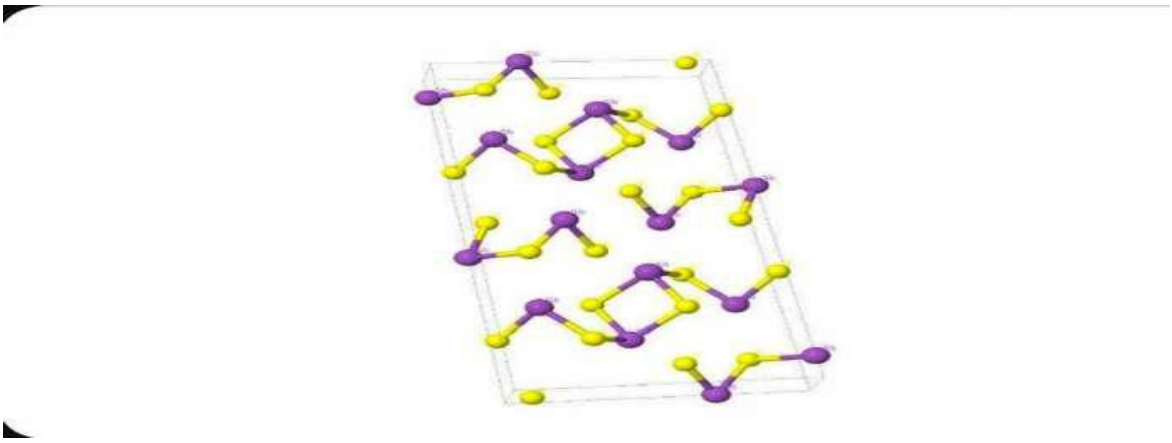

Figure II-7 Orthorhombic cristal structure of $Sb_2S(Se)_3$ compound. The yellow spheres represent S(Se) atoms while purple ones represent Sb atoms.

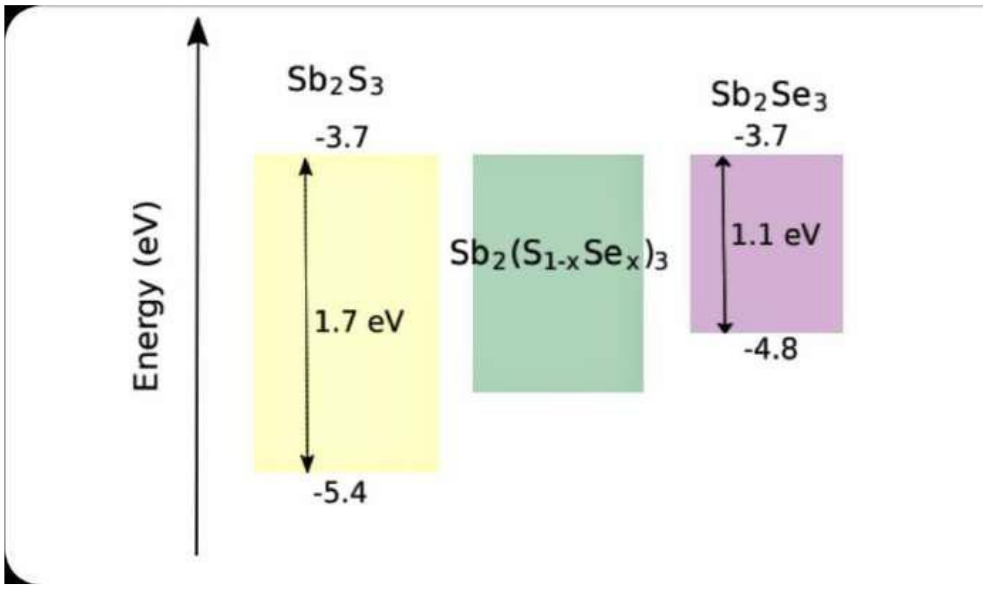

Figure II-8Band structure scheme for the $Sb_2(Se_{1-x}S_x)_3$based solar cells. The energy levels are referred to the vacuum level.

II.9. Synthesis Techniques of $Sb_2(Se_{1-x}S_x)_3$planar Thin Films and Solar Cells

The synthesis of Sb_2S_3 and Sb_2Se_3 compounds for solar cell devices has been reported employing mainly the following techniques: chemical bath deposition (CBD), thermal and rapid thermal evaporation, spin coating, vapor transport deposition, and magnetron sputtering deposition .As far as we know, the first report to produce$Sb_2(S_{1-x}Se_x)_3$material in large scale was presented by Deng et al.[37]. They synthesized for the first time $Sb_2(S_{1-x}Se_x)_3$nanotubes using a colloidal synthetic technique. They found a quadratic relationship between the band-gap of the compound and its sulfur to selenium compositional ratio, showing that changing the S concentration in the compound $Sb_2Se_{3-x}S_x$ leads to an increase in the bang-gap from 1.18 eV (the Sb_2Se_3 case) to 1.63 eV (the Sb_2S_3case), this change followed the :$E_g(x) = 0.0344x2 + 0.0481x + 1.18$ eV equation.

Furthermore, they reported the lattice constants of $Sb_2(S_{1-x}Se_x)_3$and showed that they vary linearly as a function of the sulfur concentration. Another approach for fabrication of $Sb_2(S_{1-x}Se_x)_3$based solar cells is the sequential deposition of semiconductor layers of Sb_2S_3 and Sb_2Se_3in a step-wise manner. Choi et al.[24] proposed a method to obtain efficient graded $Sb_2(S_{1-x}Se_x)_3$ absorber material through the sequential deposition of a Sb_2Se_3layer (using spin coating method), which was followed by the deposition of a Sb_2S_3layer (through CBD) onto the surface of a mesoporous TiO_2. The best device produced by this group could reach a conversion efficiency of 6.6%. The preparation of

planar hetero junction solar cells based on selenium-graded $Sb_2(S_{1-x}Se_x)_3$was reported by Zhang et al.

II.10.Conclusion

In this chapter, we review the properties and structures of Sb_2X_3 solar cells, material composition and device construction, and introduce the material $Sb_2(Se_{1-x}S_x)_3$that constitutes The basic part of the photovoltaic cell that we will study in the following Plus cell description based on $Sb_2(Se_{1-x}S_x)_3$.

Chapter III

Simulation of a photovoltaic solar cell

based on $Sb_2(Se_{1-x}S_x)_3$

Chapter III: Simulation of a photovoltaic solar cell based on $Sb_2(Se_{1-x}S_x)_3$

III.1.Introduction

Photovoltaic devices modeling is an essential tool to improve the efficiency of these (PV) cells and also to reduce manufacturing cost. These models allow a better understanding of the influence of different physical parameters on the performance of these cells, to design and optimize different types of cells without systematically resorting to experimental procedures that it can be expensive, evaluate the potential of the structure and its maximum theoretical efficiency. Several simulators for PV devices are currently available, and they are free to access or under license.

In this chapter, we will provide a brief description of the simulation method used by SCAPS software, in addition to the basic modeling equations used by this program. Then, using simulation by SCAPS software, we will study the effect of the thickness, the composition Y and the doping density Na as well as the defects density Nt of the absorber layer in $Sb_2(Se_{1-x}S_x)_3$ on the short-circuit current density voltage (Jsc), open circuit voltage (Vco), factor Figure (FF) and conversion efficiency (η) of the cell. This allowed us to derive the optimal values that give the best performance.

III.2.Device structure and simulation methodology

III.2.1. Device structure

The proposed device structure used for this simulation study is Mo/($Sb_2(Se_{1-x}S_x)_3$)/n-CdS/i-ZnO/n-ZnO: Al/ metal contact and shown in (Figure III-1), where Molybdenum (Mo) is a back contact, $Sb_2(Se_{1-x}S_x)_3$is absorber layer, CdS is wide bandgap window layer. Next to the buffer layer, highly resistive i-ZnO layer was used which is overlaid with Al-doped ZnO (ZnO:Al) layer used as a transparent conductive oxide (TCO) to collect and carry charges out of the cell. The role of the i-ZnO layer is to restrict the intermixing between the absorber and TCO layer, which in turn reduced the shunting pathways. Mo is used to collect the generated charges and works as a positive pole of the solar cell [52].

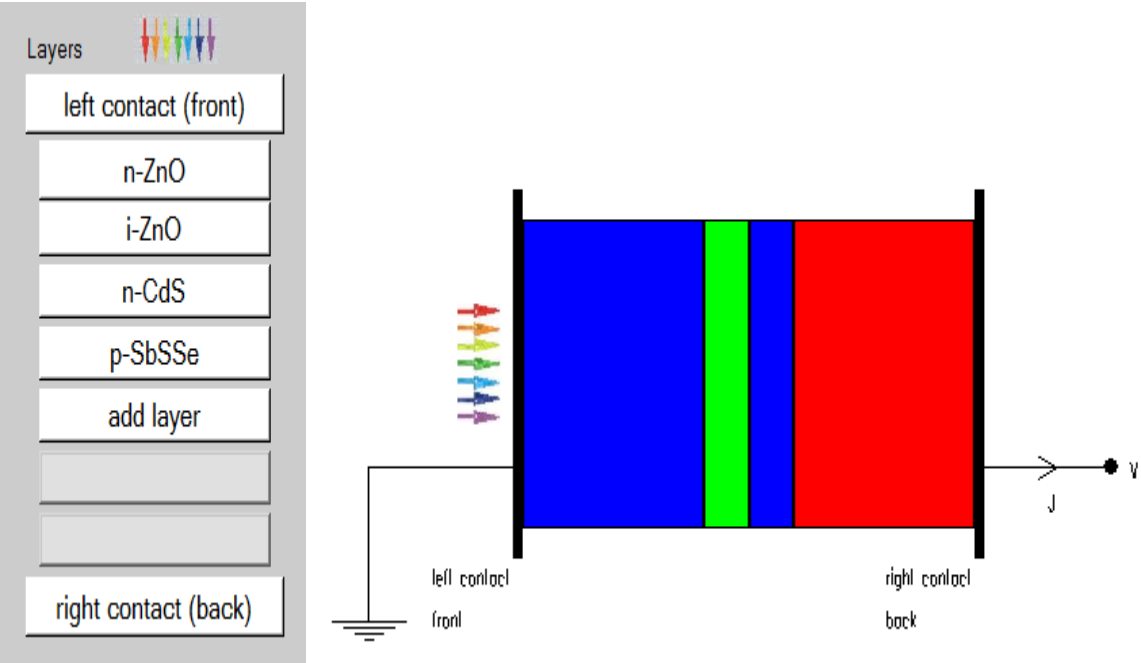

Figure III-1 The proposed device structure used in simulation

III.2.2.SCAPS-1D simulation methodology

A number of software are available which are used by several researchers to explore the performance of TFSCs like AMPS [53], SILVACO ATLAS [54], COMSOL [55], wxAMPS [56], and SCAPS [57]. In our present study, we have used SCAPS (Solar Cell Capacitance Simulator) which is a digital simulation software for solar cells, one-dimensional, developed by Department of Electronics and Information Systems of the Gent University, Belgium to simulate the performance of solar cell and its various determining parameters. The SCAPS software have several advantages like:

- Performance analysis can be done up to seven different layers.
- Recombination mechanisms: band-to-band (direct), Auger, SRH.
- Defect levels: in volume or at the interface, considering their charge states and recombination at their levels.
- Fault levels, type of load: no load (neutral), monovalent (single donor, acceptor), bivalent (double donor, double acceptor, amphoteric), multivalent (user defined).
- Defect levels, energy distribution: discrete level, uniform, Gauss, in the form of a tail or a combination.

- Defect levels, optical property: Direct excitation by the light is possible (known by photovoltaic impurity effect, IPV).
- Defect levels, meta stable transitions between levels.
- Contacts: Metal output work or flat band regime.
- Optical property (Reflection or transmission) of the filter.
- Generation: from an internal calculation or from a g(x) file provided by the user.
- Illumination: several types of spectrum are available (AM0, AM1.5D, AM1.5G, AM1.5G, Monochromatic, White, etc.).
- Illumination: on the p or n side.

The SCAPS-1D simulation tool is capable of solving three basic equations of semiconductor devices, such as Poisson's equation and the continuity equations for both electrons and holes as given below [58]:

$$\frac{\partial^2\Psi}{\partial x^2} + \frac{q}{\epsilon}[p(x) - n(x) + N_D - N_A + \rho_p - \rho_n] = 0 \quad \text{(III.1)}$$

$$\frac{1}{q}\frac{dJ_p}{dx} = G_{op}(x) - R(x) \quad \text{(III.2)}$$

$$\frac{1}{q}\frac{dJ_n}{dx} = -G_{op}(x) + R(x) \quad \text{(III.3)}$$

Where, ε is the dielectric constant, q is the electron charge, N_A and $N_D$are acceptor and donor type density respectively, Ψ is the electrostatic potential, p, n, ρ_p, ρ_n, J_p, J_n are hole concentration, electron concentration, hole distribution, electron distribution, current densities of hole and current densities of electron respectively. Gop is the optical generation rate, R is the net recombination from direct and indirect recombineation. All of these parameters are the function of the position coordinate x.

For the simulation of device structure using SCAPS-1D software several material parameters need to be included in each layer of the structure. Table 1 represents all the material parameters used for the simulation study.

All these parameters are extracted from other literature [52, 59]. For all simulation study, the illumination used was AM 1.5spectrum, 1000 W/m^2 from the front side.

Material Properties	p-Sb_2Se_3	p-Sb_2S_3	n-CdS	i-ZnO	n-ZnO
Semiconductor Property P of the pure material	A(y=0)	B(y=1)	A (y = 0)	A (y = 0)	A (y = 0)
Thickness (µm)	0.2	0.2	0.05	0.05	0.2
Acceptor Density (N_A) (cm^{-3})	10^{15}	10^{15}	0	10^{18}	0
Shallow uniform donor density N_D (cm^{-3})	0	0	10^{18}	10^{18}	10^{20}
Bandgap (eV)	1.18	1.634	2.4	3.3	3.3
Electron Affinity (eV)	4.15	3.7	4.2	4.5	4.4
Dielectric permittivity (relative)	15.1	22	10	9	9
CB effective density of states (1/cm^{-3})	10^{19}	2×10^{19}	2.2×10^{18}	2.2×10^{18}	2.2×10^{18}
VB effective density of states (1/cm^3)	10^{19}	10^{19}	1.8×10^{19}	1.8×10^{19}	1.8×10^{19}
Electron mobility (cm^2/Vs)	15	9.8	10^2	10^2	10^2
Hole mobility (cm^2/Vs)	42	10	25	25	25
Electron thermal velocity (cm^{-3})	10^7	10^7	10^7	10^7	10^7
Hole thermal velocity (cm/s)	10^7	10^7	10^7	10^7	10^7

Table III-1: Parameters of each cell layer used in the simulation.

III.3.Results and discussion

The simulation of the cell is done for uniform profiles gap of the absorber layer based $Sb_2(Se_{1-x}S_x)_3$.

III. 3. 1. Effect of absorber layer thickness

Figure III-2 below shows the variation in cell performance as a function of the absorber layer thickness type p-$Sb_2(Se_{1-x}S_x)_3$, for: Y = 0 → Eg = 1.18 eV and Na=$10^{15}cm^{-3}$and Nt = $10^{14}cm^{-3}$:

It is noted that the efficiency increases with the increase of the thickness, because if the thickness increases the absorption, and thus the generation of charge carriers also increases. This increases the current, however, the voltage and fill factor are down. The compromise is the optimal thickness value about 0.2 µm, which gives a maximum efficiency of 8.21%.

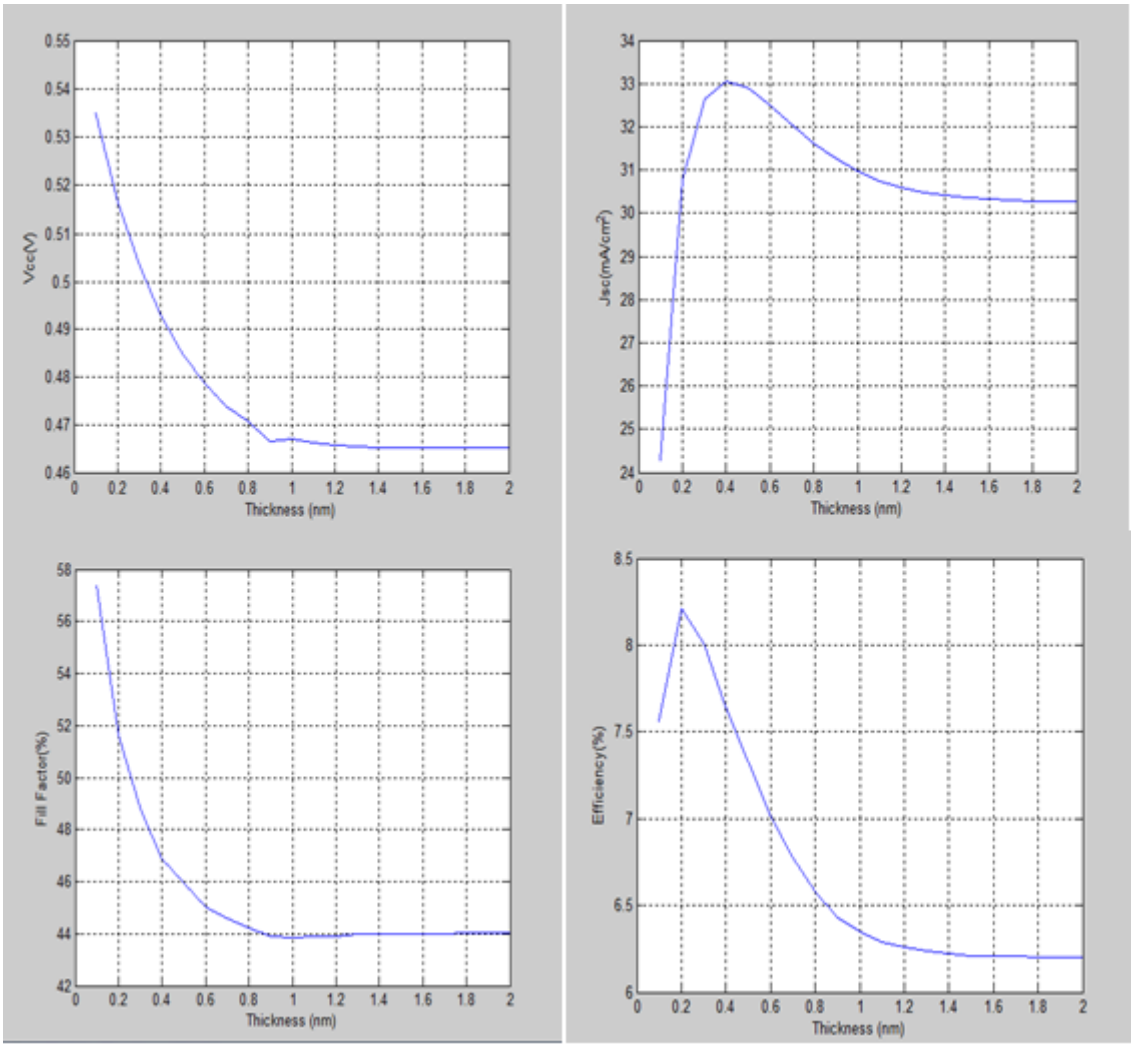

Figure III-2 Effect the absorber layer thickness$Sb_2(Se_{1-x}S_x)_3$ on the performance of the photovoltaic cell

III. 3. 2. Effect of composition Y (Bandgap Eg)

(Figure III-3) below illustrates the variation in cell performance as a function of the composition Y of the p-$Sb_2(Se_{1-x}S_x)_3$absorber layer for: Thickness = 0.2 µm and; Na= $10^{15}cm^{-3}$and Nt = $10^{14}cm^{-3}$.

The bandgap Eg depends on Y by a quadratic equation given by:

$$E_g(Y) = 0.3096.Y^2 + 0.1443.Y + 1.18 \ (eV) \qquad \text{(III.4)}$$

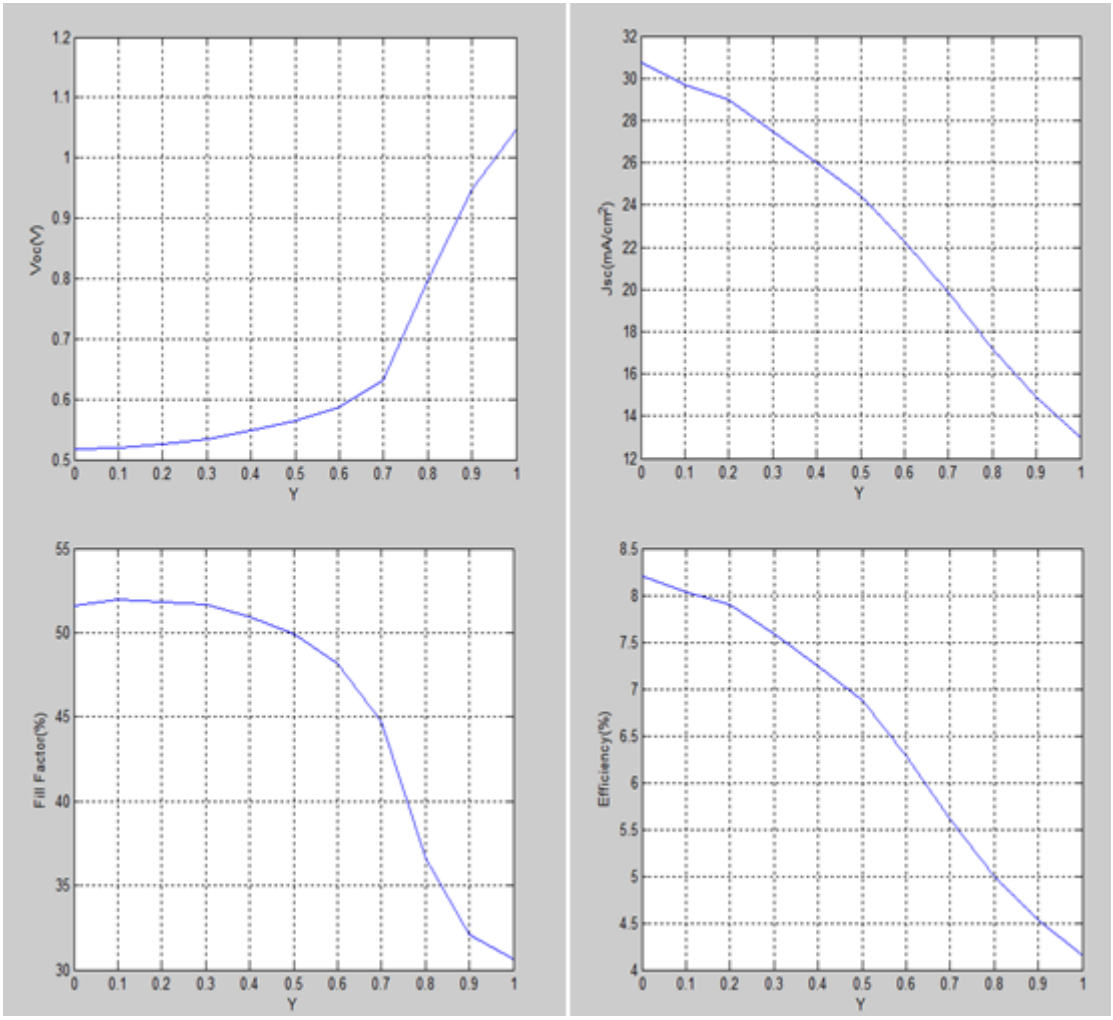

Figure III-3 Effect of the Y composition of the $Sb_2(Se_{1-x}S_x)_3$ layer on the performance of the photovoltaic cell.

According to Figure III-3, we notice that if Y (the gap Eg) increases the number of photogene rated carriers decreases, hence the decrease in current. What results from it, an optimal value of the composition Y = 0, which corresponds to a bandgap Eg = 1.18 eV. The maximum efficiency is η = 8.21%.

III. 3 .3. Effect of doping density Na

(Figure III-4) below shows the variation in cell performance as a function of the dopingsity Na of the P-type $Sb_2(Se_{1-x}S_x)_3$ absorber layer for: thickness = 0.2 µm and Nt= $10^{14}cm^{-3}$ and Y = 0.

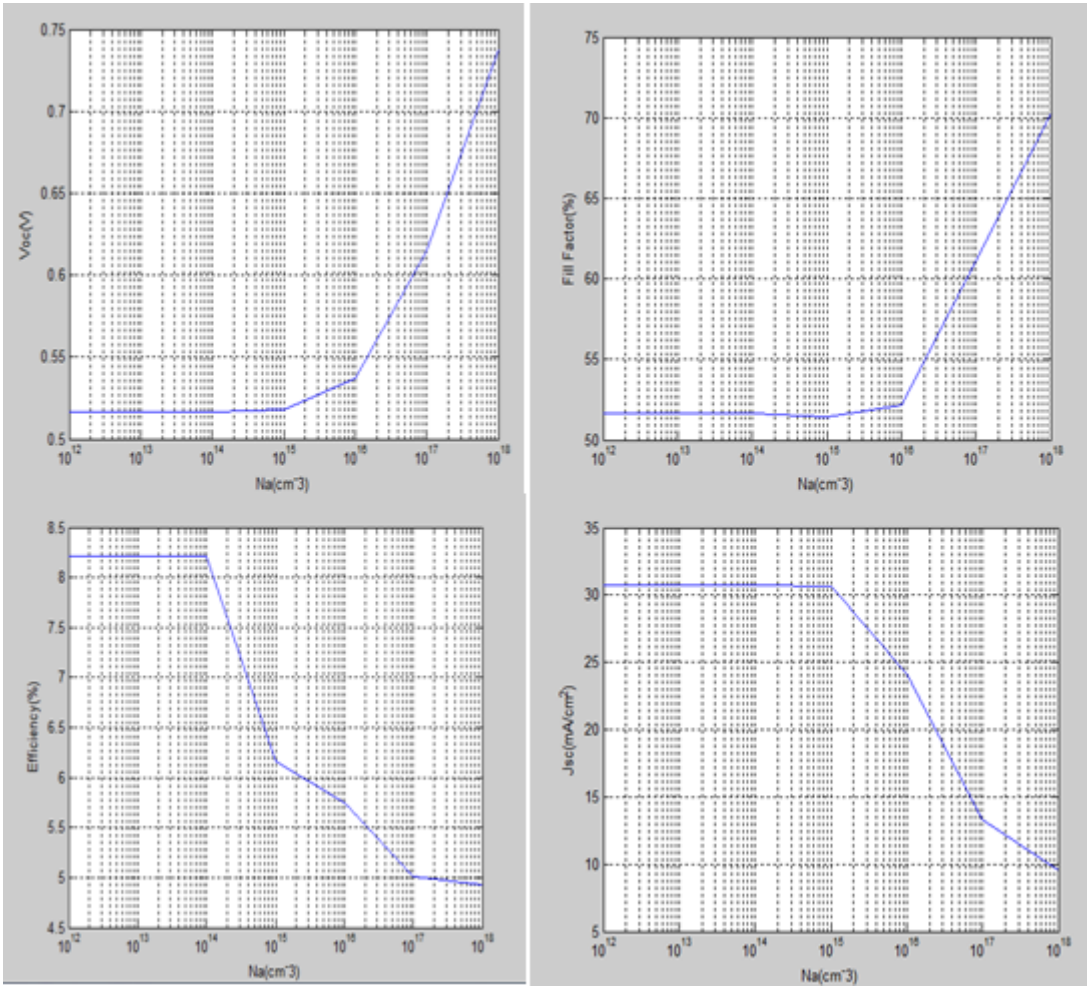

Figure III-4 Effect of doping density Na of the $Sb_2(Se_{1-x}S_x)_3$ layer on the performance of the photovoltaic cell.

As shown in (Figure III-4), cell performance is almost invariant as long as the Na doping is below $10^{14}cm^{-3}$. However, as soon as it exceeds this value, a drop in performance is observed. This allowed us to conclude that the optimal Na doping value should not exceed$10^{14}cm^{-3}$. The corresponding efficiency is η = 8.21%.

III. 3. 4. Effect of defect density Nt

(Figure III-5) below shows the variance in cell performance as a function of defect density Nt in the p-$Sb_2(Se_{1-x}S_x)_3$ absorber layer for: Wp = 0.2 µm, Na =$10^{14}cm^{-3}$, and Y= 0.

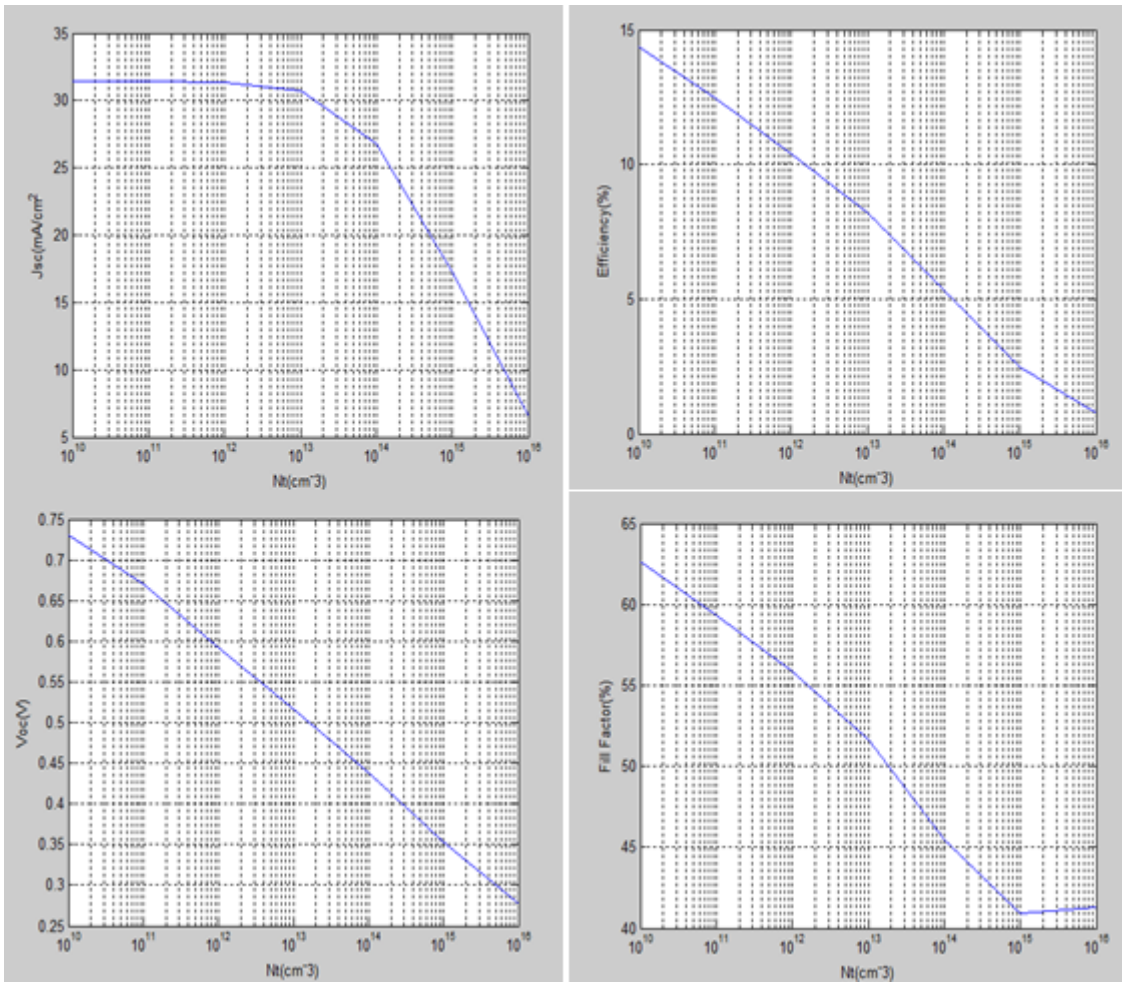

Figure III-5 Effect of defect density of $Sb_2(Se_{1-x}S_x)_3$layer on photovoltaic cell performance.

According to (Figure III-5), we note that for a good cell performance, it is essential that the absorber layer of $Sb_2(Se_{1-x}S_x)_3$has aNt defect density as low as possible.

III. 4.Conclusion

In this work, a solar cell with Mo / ($Sb_2(Se_{1-x}S_x)_3$)/ n-CdS / i-ZnO/ n-ZnO structure was modeled and simulated using SCAPS-1D software to obtain the optimized parameters of the device which will helps us to achieve better photo conversion efficiency. Many controllable parameters that affect performance have been improved such as thickness, bandgap, doping density and defect density of the absorber layer. A maximum efficiency of 8.21% is obtained.

General conclusion

General conclusion

This research work is based on numerical simulation in order to optimize the absorber layer $Sb_2(Se_{1-x}Sx)_3$ of a thin film photovoltaic solar cell having the following structure: n-ZnO / n-CdS / i-ZnO / p-$Sb_2(Se_{1-x}Sx)_3$.

The simulation is done using SCAPS software. SCAPS allows us to extract a various cell parameters such as: short-circuit current density, J_{SC}, Open circuit voltage, V_{CO}, fill factor, FF and conversion efficiency η.

This simulation leads us to the following main results:

- ✓ The thickness of the absorbent layer $Sb_2(Se_{1-x}Sx)_3$should have an optimal value of about 0.2 μm;
- ✓ The best efficiency is obtained for the optimum value of the lowest composition Y = 0 which corresponds to the lowest bandgap Eg = 1.18 eV;
- ✓ The optimum doping density value should not exceed 10^{15} cm^{-3};
- ✓ The absorber layer $Sb_2(Se_{1-x}Sx)_3$ should have the lowest possible defect density.

All these optimal values give a maximum efficiency η = 8.21%

Bibliography

Bibliography

[1] V. Quaschning, Understanding renewable energy systems, Earthscan, London,2005.

[2] HG. N. Tiwari, Solar Energy, Fundamentals, Design, Modelling and Applications, Narosa, Publishing House, New Delhi, India, 2004.

[3] N. Duncan and K. S. Robert, 'The Canadian Renewable Energy Guide', Burns town, General Store Publishing House, 1995.

[4] A. Aziz et al., 'Modélisation des Panneaux Solaires dans l', Environnement Orcad.

[5] A. Ricaud, 'Modules photovoltaïques : Filières technologiques', Techniques de l'ingénieur. Génie électrique, vol. 7, no. D3940, 2005.

[6] B. G. Streetman and S. Banerjee, Solid state electronic devices, vol. 2. Prentice-Hall Englewood Cliffs, NJ, 1995.

[7] N. Yamamoto, S. Noda, and A. Sasaki, 'New realization method for three-dimensional photonic crystal in the optical wavelength region: experimental consideration', Japanese journal of applied physics, vol. 36, no. 3S, p. 1907, 1997.

[8] E. Özbay et al., 'Double-etch geometry for millimeter-wave photonic band-gap crystals', Applied physics letters, vol. 65, no. 13, pp. 1617–1619, 1994.

[9] M. Grätzel, 'Dye-sensitized solar cells', Journal of Photochemistry and Photobiology C: Photochemistry Reviews, vol. 4, no. 2, pp. 145–153, 2003.

[10] S. Astier, Conversion photovoltaïque : du rayonnement solaire à la cellule. Ed. Techniques de l'ingénieur, 2008.

[11] F. Lasnier, Photovoltaic engineering handbook. CRC Press, 1990.

[12] H. Mathieu and H. Fanet, Physique des semiconducteurs et des composants électroniques-6ème édition: Cours et exercices corrigés. Dunod, 2009.

[13] B.Godfrey, Renewable Energy Power for a Sustainable Future, **78**, (2004).

[14] http://www.docstoc.com/docs/95721473/Solar-Energy-Presentation-0220

[15] http://www.zhengneng.com/enproduct_139.html

[16] M. A. Green, E.D.Dunlop, J. Hohl-Ebinger, M. Yoshita,N.Kopidakis, X. Hao, Prog. Photovoltaics 2020, 28, 629.

[17] C. Chen, J. Tang, ACS Energy Lett. 2020, 5, 2294.

[18] H. Lei, J. Chen, Z. Tan, G. Fang, Sol. RRL 2019, 3, 1900026.

[19] X. Wang, R. Tang, C. Jiang, W. Lian, H. Ju, G. Jiang, Z. Li, C. Zhu, T. Chen, Adv. Energy Mater. 2020, 10, 2002341.

[20] Y. C. Choi, D.U. Lee, J. H.Noh, E. K. Kim, S. I. Seok, Adv. Funct. Mater. 2014, 24, 3587.

[21] J. Han, S. J. Wang, J. B. Yang, S. H. Guo, Q. Cao, H. J. Tang, X. Y. Pu, B. Y. Gao, X. H. Li,ACS Appl. Mater. Inter 2020, 12, 4970.

[22] Z. Li, X. Liang, G. Li, H. Liu, H. Zhang, J. Guo, J. Chen, K. Shen, X. San,W. Yu, Nat. Commun. 2019, 10, 1.

[23] Y. C. Choi, T. N. Mandal, W. S. Yang, Y. H. Lee, S. H. Im, J. H.Noh, S. I. Seok, AngewandteChemie 2014, 126, 1353.

[24] Y. C. Choi, Y. H. Lee, S. H. Im, J. H. Noh, T. N. Mandal, W. S.Yang, S. I. Seok, Adv. Energy Mater. 2014, 4, 1301680.

[25] Dong, J., Liu, Y., Wang, Z., & Zhang, Y. (2021). Boosting VOC of antimony chalcogenide solar cells: A review on interfaces and defects. Nano Select, 2(10), 1818-1848.

[26] B. Lee, J. He, R. P. Chang, M. G. Kanatzidis, Nature 2012, 485, 486.

[27] U. Bach, D. Lupo, P. Comte, J.-E. Moser, F. Weissörtel, J. Salbeck, H. Spreitzer, M. Grätzel, Nature 1998, 395, 583.

[28] L. Calio, S. Kazim, M. Graetzel, S. Ahmad, Angew. Chem. Int. Ed. 2016, 55, 14522.

[29] H. Lei, J. Chen, Z. Tan, G. Fang, Sol. RRL 2019, 3, 1900026.

[30] Y. Zhou, M. Leng, Z. Xia, J. Zhong, H. Song, X. Liu, B. Yang, J. Zhang, J. Chen, K. Zhou, Adv. Energy Mater. 2014, 4, 1301846.

[31] L. Wang, D.-B. Li, K. Li, C. Chen, H.-X. Deng, L. Gao, Y. Zhao, F. Jiang, L. Li, F. Huang, Nat. Energy 2017, 2, 1.

[32] L. Liu, S. Zhang, J.Wu,W.Wang,W. Liu, L.Wu,Y. Zhang, Chin.Phys. B 2020, 29, 058801

[33] X. Wang , J. Li , W. Liu , S. Yang , C. Zhu , T. Chen , Nanoscale 9 (2017) 3386–3390. 18.Y.C. Choi , T.N. Mandal , W.S. Yang , Y.H. Lee , S.H. Im , J.H. Noh , S.I. Seok , Angew. Chem. Int. Ed. 53 (2014) 1329–1333

[34] Y.C. Choi , T.N. Mandal , W.S. Yang , Y.H. Lee , S.H. Im , J.H. Noh , S.I. Seok , Angew. Chem. Int. Ed. 53 (2014) 1329–1333

[35] G.-Y. Chen , B. Dneg , G.-B. Cai , T.-K. Zhang , W.-F. Dong , W.-X. Zhang , A.-W. Xu , J. Phys. Chem. C 119 (2008) 672–679 .

[36] B.B. Nayak , H.N. Acharya , T.K. Chaudhuri , G.B. Mitra , Thin Solid Films 92 (1982) 309–314 .

[37] G.-Y. Chen , W.-X. Zhang , A.-W. Xu , Mater. Chem. Phys. 123 (2010) 236–240 .

[38] Q. Xie , Z. Liu , M. Shao , L. Kong , W. Yu , Y. Qian , J. Cryst. Growth 252 (2003) 570–574 .

[39] O. Savadogo , K.C. Mandal , J. Phys. D Appl. Phys. 27 (1994) 1070–1075 .

[40] J. George , M.K. Radhakrishnan , J. Phys. D Appl. Phys. 14 (1981) 899–905 .

[41] T. Englman , E. Terkieltaub , L. Etgar , J. Phys. Chem. C 119 (2015) 12904–12909 .

[42] O. Savadogo , K.C. Mandal , J. Electrochem. Soc. 139 (1992) L16–L18 .

[43] Y. Itzhaik , O. Niitsoo , M. Page , G. Hodes , J. Phys. Chem. C 113 (2009) 4254–4256

[44] X. Wang et al., Development of antimony sulfide–selenide $Sb_2(S,Se)_3$ -based solar cells, Journal of Energy Chemistry 27 (2018) 713–721.

[45] N. Guijarro, T. Lutz , T. Lana-Villarreal , F. O'Mahony , R. Gomez , S.A. Haque , J. Phys. Chem. Lett. 3 (2012) 1351–1356 .

[46] Z. Li , H. Zhu , Y. Guo , X. Niu , X. Chen , C. Zhang , W. Zhang , X. Liang , D. Zhou , J. Chen , Y. Mai , Appl. Phys. Express 9 (2016) 052302 .

[47] M. Leng , M. Luo , C. Chen , S. Qin , J. Chen , J. Zhong , J. Tang ,Appl. Phys. Lett. 105 (2014) 083905 .

[48] Y. Zhou , L. Wang , S. Chen , S. Qin , X. Liu , J. Chen , D.-J. Xue , M. Luo , Y. Cao , Y. Cheng , E.H. Sargent , J. Tang , Nat. Photonics 9 (2015) 409–415 .

[49] Z. Li , X. Chen , H. Zhu , J. Chen , Y. Guo , C. Zhang , W. Zhang , X. Niu , Y. Mai , Sol. Energy Mater. Sol. Cells 161 (2017) 190–196 .

[50] B. Yang , S. Qin , D.-j. Xue , C. Chen , Y.-S. He , D. Niu , H. Huang , J. Tang , Prog. Photovolt. Res. Appl. 25 (2017) 113–122 .

[51] Thalía Jiménez, C. I. León-Pimentel,b Diego Seuret-Jiménez, and MaykelCourel. State of the Art on $Sb_2(S_{1-x},Se_x)_3$ Thin Film Solar Cells. Gen. Chem. 2019, 5, 180029

[52] Lhoussayne Et-taya, TouriaOuslimane, AbdellahBenami, Numerical analysis ofearth-abundant $Cu_2ZnSn(S_xSe_{1-x})_4$ solar cells based on Spectroscopic Ellipsometryresults by using SCAPS-1D, Sol. Energy 201 (2020) 827–835, https://doi.org/10.1016/j.solener.2020.03.070

[53] Y.Z. Hamri, Y. Bourezig, M. Medles, M. Ameri, K. Toumi, I. Ameri, Y. Al Douri, C.H. Voon, Improved efficiency of Cu(In,Ga)Se_2 thin film solar cells using a bufferlayer alternative to CdS, Sol. Energy 178 (2019) 150–156, https://doi.org/10.1016/j.solener.2018.12.023

[54] A. Hima, N. Lakhdar, B. Benhaoua, A. Saadoune, I. Kemerchou, F. Rogti, Anoptimized perovskite solar cell designs for high conversion efficiency, Superlattice.Microst. 129 (2019) 240–246, https://doi.org/10.1016/j.spmi.2019.04.007

[55] S. Zandi, P. Saxena, N.E. Gorji, Numerical simulation of heat distribution in RGOcontactedperovskite solar cells using COMSOL, Sol. Energy 197 (2020) 105–110,https://doi.org/10.1016/j.solener.2019.12.050

[56] A. Bag, R. Radhakrishnan, R. Nekovei, R. Jeyakumar, Effect of absorber layer, holetransport layer thicknesses, and its doping density on the performance ofperovskite solar cells by device simulation, Sol. Energy 196 (2020) 177–182,https://doi.org/10.1016/j.solener.2019.12.014

[57] ImanGharibshahian, Ali A. Orouji, SamanehSharbati, Towards high efficiency Cd-Free Sb_2Se_3 solar cells by the band alignment optimization, Sol. Energy Mater. Sol.Cells 212 (2020) 110581, https://doi.org/10.1016/j.solmat.2020.110581

[58] A. Benami, Effect of CZTS parameters on photovoltaic solar cell from numericalsimulation, J. Energy Power Eng. 13 (2019) 32–36, https://doi.org/10.17265/1934-8975/2019.01.003.

[59] M.T. Islam, A.K. Thakur, Two stage modelling of solar photovoltaic cells based onSb_2S_3 absorber with three distinct buffer combinations, Sol. Energy 202 (2020)304–315, https://doi.org/10.1016/j.solener.2020.03.058.

Appendix

Appendix. A: SCAPS program

A.1. Simulation parameters

In order to simulate and control all parameters of the photovoltaic device

With the SCAPS program, we have to go through three large windows:

- ❖ Execution window ("Work board").
- ❖ Device design window and problem definition (definition Team).
- ❖ Results window.

A. 2. Storyboard

First by running the application, the execution window which is the menu

Main opens. The window that opens is shown in Figure A-1.

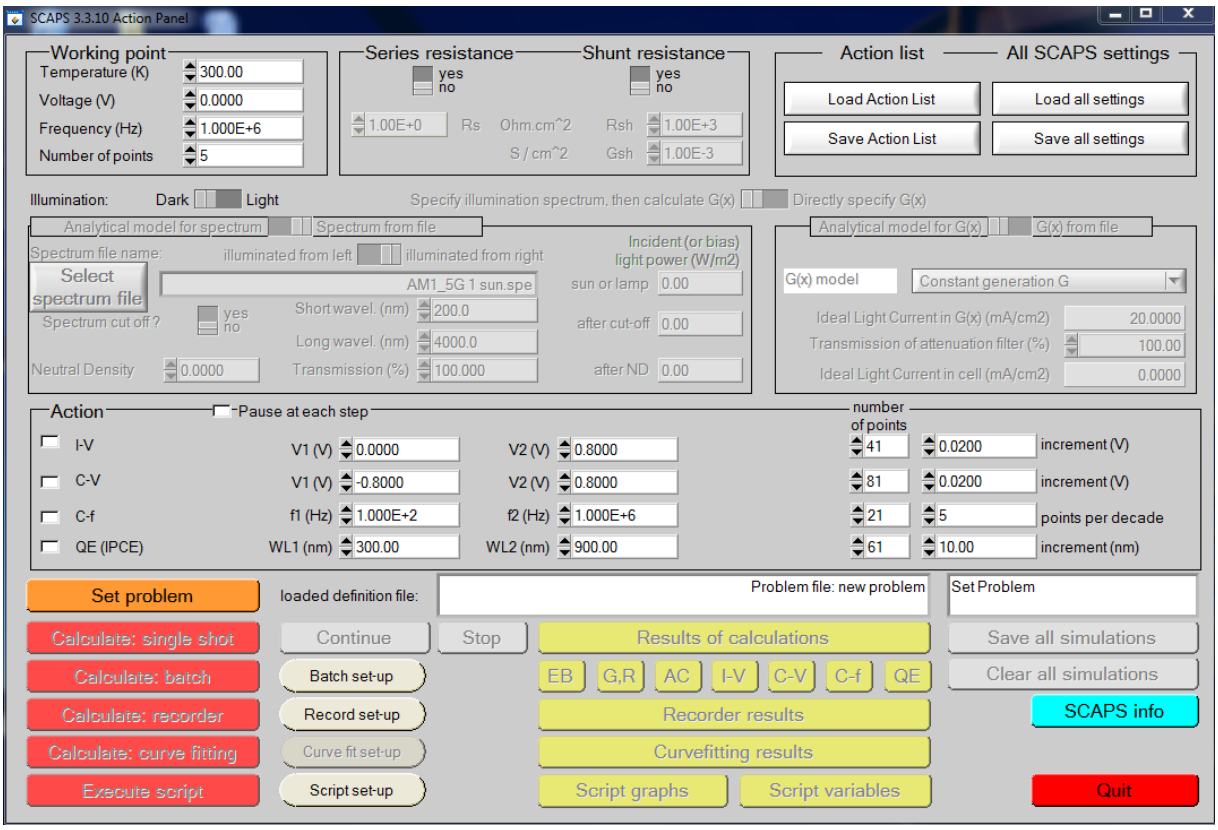

Figure A.1: SCAPS start panel, the action or main panel

A. 3. Define the problem

We click on the SET PROBLEM button in the action panel, and we choose

LOAD in the lower right corner of the panel that opens afterwards.

A. 4. Determine the operating point

The operating point defines the non-variable parameters in Simulation measurements, which are related to the measurement process. This means:

- **Temperature T**: The temperature of the cell or device PV.
- **Voltage V:** Not related to I-V and C-V simulations. it's the DC bias voltage in C-f and QE simulations (h). SCAPS It always starts at 0V, and operates at a point voltage

The process has a number of steps that must also be defined.

- **Frequency f:** Not related to I-V, QE (λ) and Cf simulations.

This is the frequency at which the C-V characteristic is simulated.

- **Lighting:** You can control the lighting parameters with Through specific areas, namely: activating the light source Monochromatic or polychromatic spectrum and wavelengths Including solar energy etc.....

A. 5. Selection of the characteristics to be simulated

In the Action part of the panel, you can choose one or more measures to simulate: I-V, C-V, C-f and QE (λ). You can also adjust the initial values and endings of the argument, as well as the number of steps.

A. 6. Device design window and problem definition

You can create new optical space devices through specific fields, namely

- Add a layer a window displays when the user click on this button. it contains several parameters such as energy of gap, electric permittivity, affinity, doping,

type of doping, that the user can directly use standard values in the software data files;

- Right and left adjustment (right and left contact): modify the optical and electrical parameters of the right and left outer surfaces of the cell;
- **Numerical setting:** modify the parameters digital display of the error message graphs and the convergence.

A. 7. Result of the simulation (characteristic I(V))

Executor the simulation "calculate", noted the simulation results (Icc, Vco, FF, η) in the "I-V panel" window. These results can be displayed and copied in the form of a table by pressing "show".

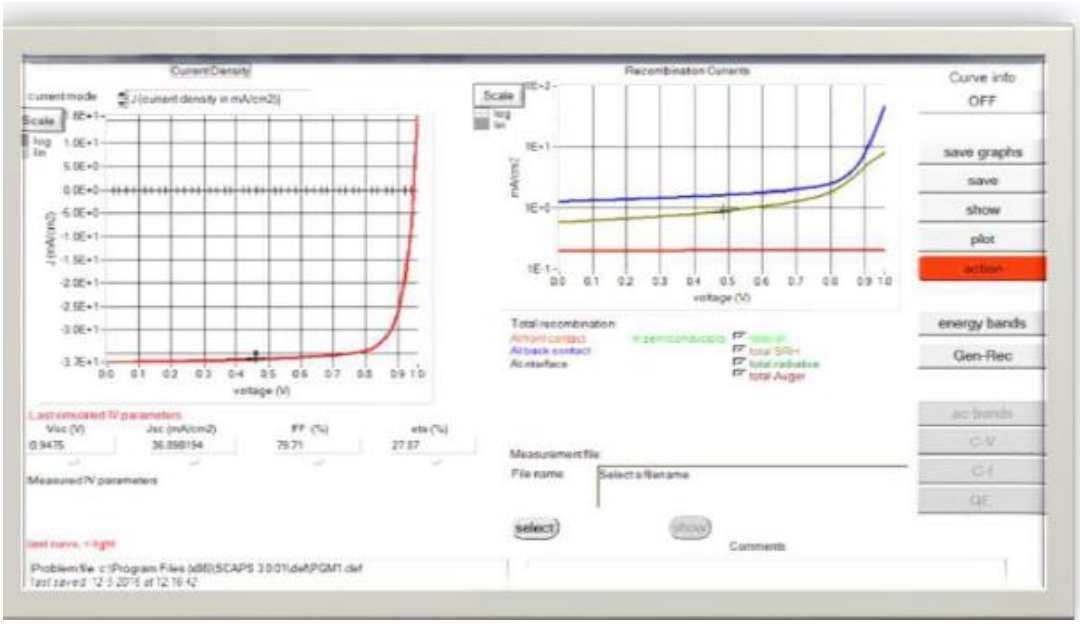

Figure A.2: Display panel of J-V curves in darkness and in illumination